March 1989 LRP 372/89

Papers contributed to the
16th EUROPEAN CONFERENCE ON CONTROLLED
FUSION AND PLASMA HEATING

Venice, Italy, March 1989

CENTRAL MASS FEEDBACK CONTROL USING THE DISCRETE ALFVEN WAVE SPECTRUM

Th. Dudok de Wit, A.A. Howling, J.B. Lister, Ph. Marmillod

Centre de Recherches en Physique des Plasmas
Association Euratom - Confédération Suisse
EPFL, Lausanne (Switzerland)

Introduction Discrete Alfvén Waves (DAW) in TCA plasmas have been well documented both experimentally and theoretically [1]. Their dispersion relation depends on several important internal plasma parameters, such as the *central effective mass*, for which no other measurement technique has yet been developed.

By frequency tracking a single DAW during a current flat-top, we obtained a real-time estimate of the central effective mass. Using this measurement, we have been able to feedback control both the effective mass and the electron density of the plasma.

Theoretical background The shear Alfvén wave dispersion relation is given by :

$$\omega^2(r) = \left(\frac{B_o^2}{\mu_o \rho(r)}\right) \frac{(n + \frac{m}{q(r)})^2}{R_o^2} \left(1 - \frac{\omega^2(r)}{\omega_{ci}^2}\right) \qquad 1)$$

where n, m are respectively the toroidal and poloidal wavenumbers, $\rho(r) = n_e(r)\, A_{eff}(r)\, m_p$ the mass density and m_p the proton mass.
Since we have $\omega_{DAW} \approx \min \omega(r) \approx \omega(r=0)$ and assuming $\omega^2 \ll \omega^2_{ci}$, this becomes :

$$\omega^2_{DAW} \sim \frac{(n + \frac{m}{q(0)})^2}{A_{eff}(0)\, n_e(0)} \qquad 2)$$

Some common values for A_{eff} are 1 for hydrogen, 2 for deuterium and most fully stripped impurities, 3 for tritium only.

Results from a 1-D simulation code fully confirm 2). However, particular attention must be paid to several parameters that may modify the approximate form of the DAW dispersion relation and which do not appear explicitly here, such as: a) the plasma current and its profile (other than q(0)); b) the density profile (other than $n_e(0)$); c) the position of the magnetic axis.

Experimental setup The diagnostic uses a small double-bar antenna situated on the outer equatorial midplane mounted on a rotating flange which allows it to be tilted with respect to the magnetic field lines. This antenna is fed by a 100W amplifier which provides an oscillatory current up to 15 A via a wideband matching circuit in the 1-6

MHz range. The system (fig. 2) has been designed to operate ultimately together with the high power Alfvén wave heating of TCA.

The plasma response to the excitation is detected by an RF pickup coil which gives the toroidal wavefield component $b\phi$, both in amplitude and in phase. Alfvén resonances are easily identified by amplitude peaks and phase rotations of 360°. Since the phase changes rapidly during a resonance, a phase-locked loop can be used to track a peak [2]. Earlier results [3,4] have proven this method to be sufficiently accurate to track a DAW with a bandwidth up to 10 kHz.

Once we know the DAW frequency and the mode numbers (n,m), the effective mass, or rather its inverse, can be computed in real time using a set of analog multipliers. For real-time calculations, the central electron density is approximated by taking the line-averaged density signal and multiplying it by a constant. This may introduce a small error when sudden gas puffs temporarily broaden the density profile, but this could ultimately be compensated.

Next, we feedback control both the plasma effective mass and the electron density. A 2-input, 2-output feedback loop (fig. 3) compares the analog signals $1/A_{eff}$ and $\bar{n}_e$ with two values programmed by the operator. The resulting errors ε are crosscoupled and the outputs act separately on both the hydrogen and deuterium gas valves.

<u>Temporal evolution of the effective mass</u> We tested the mass control system by running it with several different target values. It works well provided that the target density can be reached smoothly. Reasonable ranges are $\bar{n}_{e19}>1.5$ and $A_{eff}=1.2–2$. An absolute calibration of A_{eff} was carried out in a deuterium conditioned vessel, in which case the effective mass the least sensitive to impurity concentrations, and thus as close as possible to 2. Subsequently, all experiments were run during the current flat-top (I_p=130 kA, q(a)=3.1, (n,m)=(–2,–1) or (–1,–1)). The error on the measured effective mass for a single shot is estimated to be less than 3%.

We studied the temporal evolution of A_{eff} by puffing hydrogen into deuterium plasmas. The values of A_{eff} and $\bar{n}_e$ may be used to estimate the gas recycling rate at the centre of the plasma. Fig. 1 presents a shot with mass control, during which both A_{eff} and $\bar{n}_e$ evolve asymptotically towards the preset target values. The offset errors and the relatively low convergence time ($\tau \approx 7$ ms) can be reduced by optimizing the PI control circuits.

<u>Conclusion</u> We report the first attempt to estimate and control the plasma central effective mass by tracking the frequency of a global Alfvén eigenmode. The control system is easy to use, although several internal plasma parameters must be taken into account. Since deuterium and tritium have different effective masses, the diagnostic also offers a way to measure D-T mixtures in next generation tokamaks.

Acknowledgements : We are grateful for the continuous support of the TCA team in carrying out this study, which was partly funded by the Fonds National Suisse de la Recherche Scientifique.

References

[1] G.A. COLLINS *et al.*(1986), Phys.fluids **29**, 2260

[2] Equipe TFR (1977), Proc. of the Sixth Int. Conf. on Plasma Physics and Controlled Nuclear Fusion Research, IAEA, Berchtesgaden, III, 39

[3] G.A. COLLINS *et al.*(1987), Plasma Phys. Contr. Fusion **29**, 323

[4] G.A. COLLINS *et al* (1987), Plasma Phys. Contr. Fusion **29**, 1631.

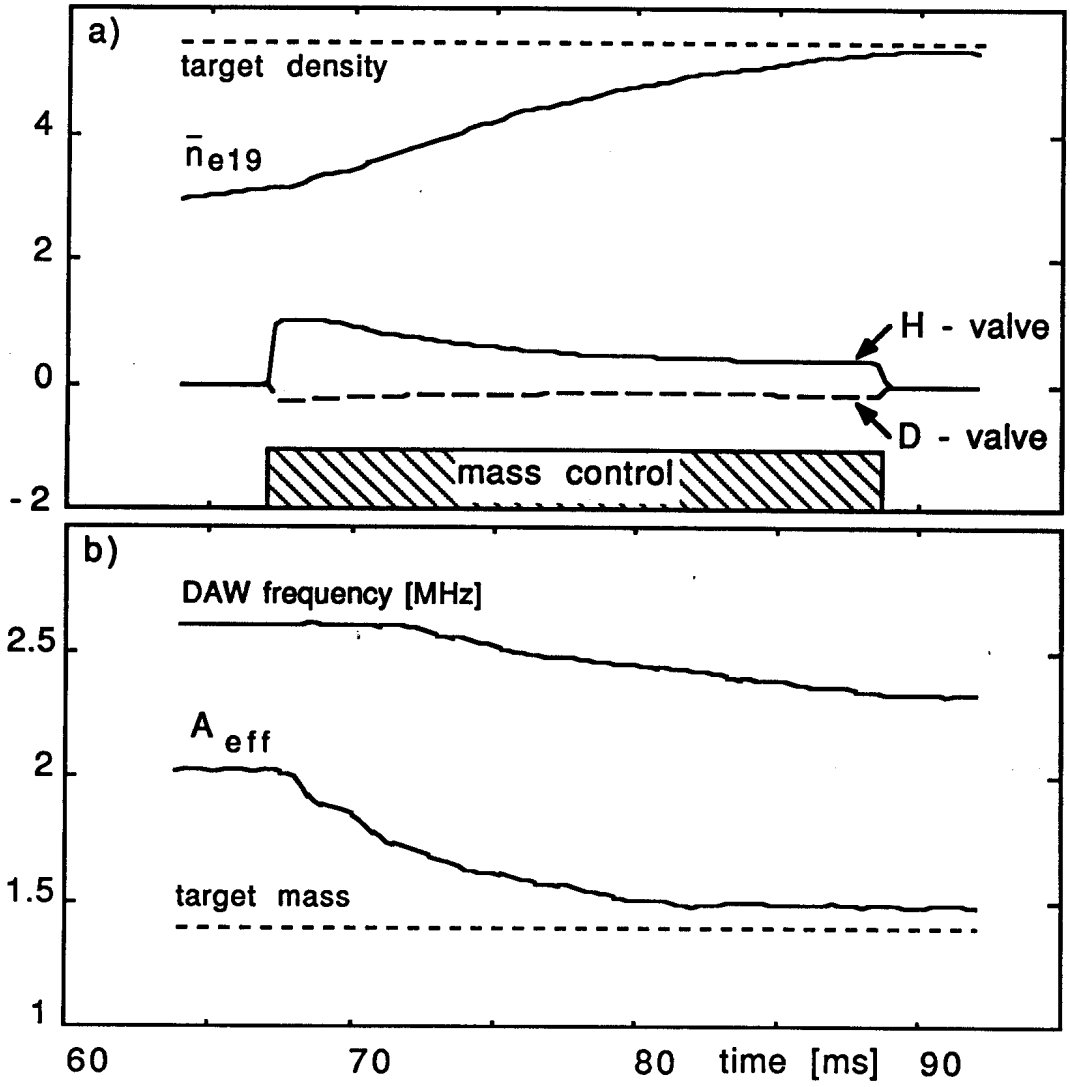

Figure 1 Shot with both density and mass control working between t=67 and 89 ms. Tha plasma initially contains only deuterium. In a), the hydrogen gas input is approximately proportional to the valve signal, whereas the deuterium valve remains closed. The target density and effective mass are reached respectively with an error of 3% and 7% (#28351, 130kA).

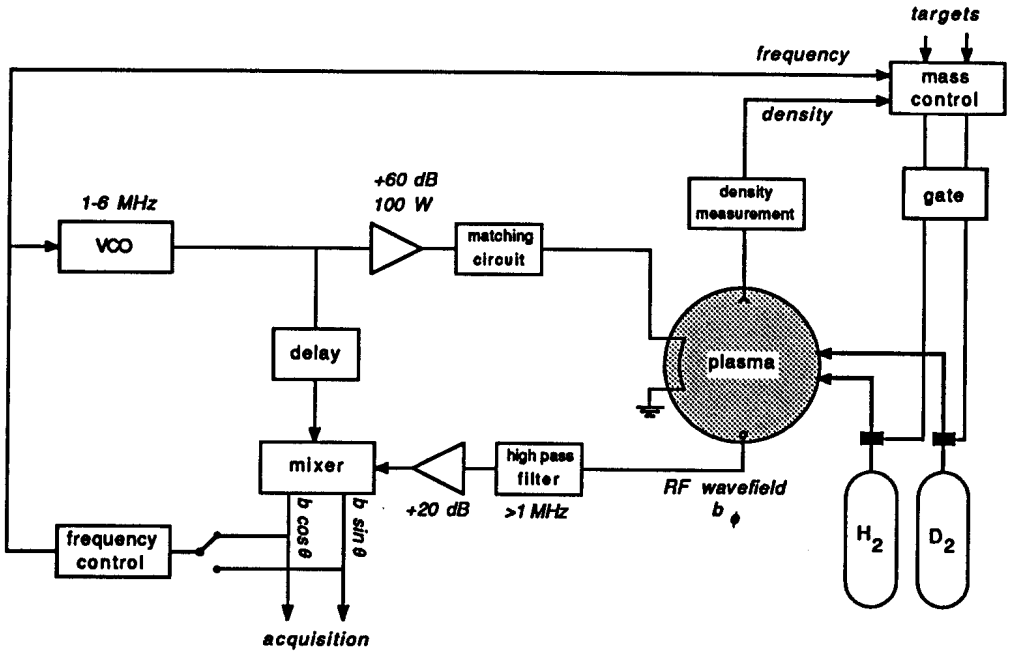

Figure 2 : The frequency tracking and mass control circuits

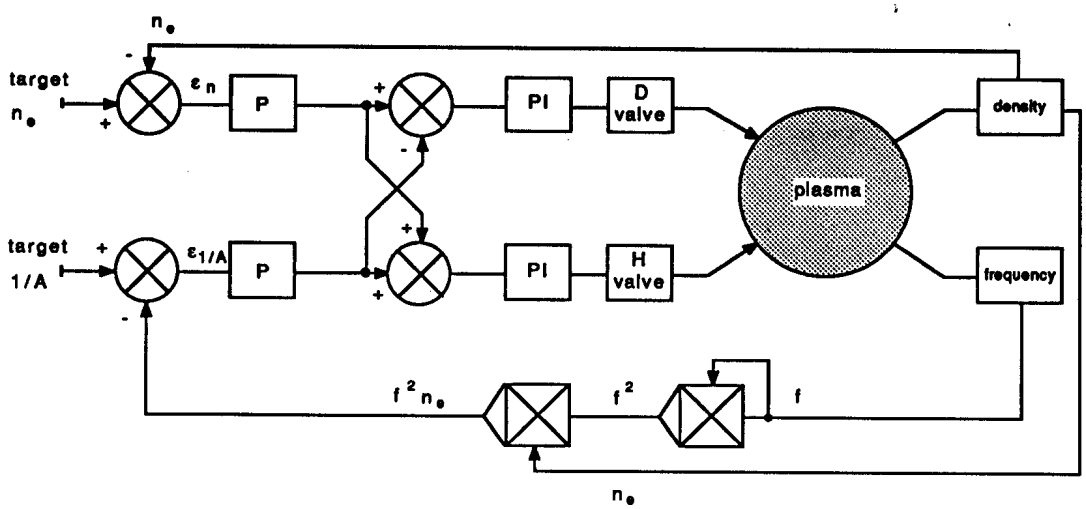

Figure 3 : Mass control schematic layout

ANTENNA PLASMA INTERACTION AND HARMONIC GENERATION IN ALFVEN WAVE HEATING

G.G. Borg, S. Dalla Piazza, Y. Martin, A. Pochelon, F. Ryter and H. Weisen

Centre de Recherches en Physique des Plasma, Association Euratom-Confédération Suisse
Ecole Polytechnique Fédérale de Lausanne
21, Av. des Bains, CH-1007 Lausanne, Switzerland

*Max-Planck-Institut fur Plasmaphysik, D-8046 Garching, Munich, F.R.G.

Introduction Additonal plasma heating by Alfven waves (AWH) has been studied on TCA for some years. Although considerable agreement between fundamental wave and coupling phenomena has been observed [1,2], the heating results have always been poor and difficult to interpret. Only recently has energy deposition within the plasma been shown to be determined mostly by the density rise [4] and ohmic effects and not by Alfven resonant absorption within the plasma [3].

In TCA, the standard AWH antennae are unshielded and are in direct contact with the plasma scrape off layer (SOL) in the shadow of the limiter. In this paper we test the hypothesis that a Langmuir current (resistive and capacitive [5]), henceforth referred to as the default current, flows from the antennae to the plasma on application of RF potential and we estimate the parasitic power deposited at the plasma SOL interface.

Experiment In TCA there are four pairs of antennae spaced at 90^0 intervals around the machine. In each pair there is one antenna on top and one on the bottom of the plasma. AWH is normally effected by applying approximately 30kW of RF power per antenna at 2.04 MHz. If desired, these antennae can be artificially polarised negatively with respect to machine earth by a biasing circuit coupled to the antenna RF lines. One of the TCA antennas is shown in Fig. 1. We monitor the current entering each terminal of one of its three bar pairs by Rogowski coils. In addition, we monitor the RF potential with respect to the machine earth by one voltage divider on each terminal. The signals obtained are therefore proportional to the time derivatives of the current and the voltage. Under normal conditions and according to the prescription for AWH, a large antenna current, the circulating current, flows in one terminal, through the antenna bars, and out the other terminal. If a default current flows from the antenna into the plasma then the current entering one terminal of the antenna is no longer

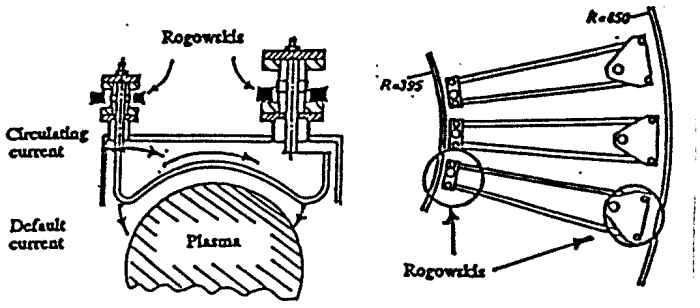

Fig. 1 AWH antenna showing the paths of the circulating current and the default currents for symmetric excitation.

equal to the current leaving the other terminal. Subtraction of the two Rogowski signals therefore permits a measurement of the default current, which must flow from the high power generator, through the terminals of the antenna, and into the SOL.

Under normal conditions the TCA antennae are excited symmetrically at RF with respect to machine earth (the terminals of the antenna are excited in push-pull) and are electrically floating at DC with respect to the plasma. The default currents entering each terminal of the antenna should then be more or less equal. Since these currents consist mainly of a rectified electron current flowing in each terminal on positive half-cycles of the terminal voltage, we predicted a default current signal at the second harmonic of the Alfvén generator frequency (2.04 MHz). The prediction was confirmed by an experiment in which a top and a bottom pair of antennae were excited (Fig 2a). The signal waveform obtained is independent of the chosen antenna poloidal phasing. The magnitude of the default current is typically 0.02 to 0.05 of the circulating antenna current for our conditions. This could explain a substantial part of the measured Alfvén power if the individual default currents flowing in both terminals are in phase with their terminal voltages, as will be shown later, and the other, unmonitored, bar pairs have similar default currents.

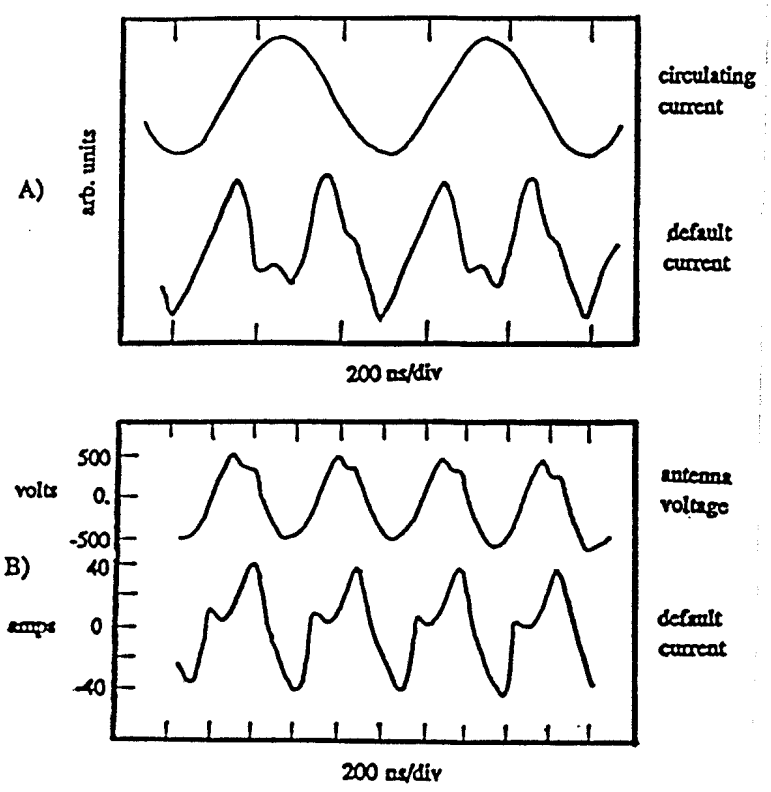

Fig. 2 Typical signal traces showing the time derivatives of the antenna potential, the circulating current and the default current.
a) Symmetric excitation.The default current trace shows the sum of the default currents entering at both antenna terminals.
b) Asymmetric excitation with one side of the antenna at machine earth.
The signals are calibrated for the first harmonic at 2.04 MHz.

The default current has some interesting properties. Firstly, the current drawn from the plasma by a passive antenna circuit when RF is applied at another toroidally separated antenna is of the same order as the directly excited default current measured on the excited antenna. This means that different antennae interact. Indeed, observation of the default current of one antenna whilst all eight antennae were excited revealed a very complicated waveform consisting of mainly first and second harmonic signals. Second, in the case of relatively high power excitation, the default current does not depend on the artificial polarisation applied to the antenna when this polarisation is more negative than the natural polarisation. According to simple floating probe theory, an oscillating potential applied to a floating metallic object in a plasma will draw a DC current until the object has charged sufficiently negative to equalise the average ion and electron currents on each half-cycle [6]. This is similar to the technique of grid-leak bias used in circuits involving electron tubes. If a more negative potential is applied to the object, then any increase in RF current must be due to an ion current which causes a DC current to flow to the polarisation source. This increase in RF current is small due to the low ion thermal velocity.

It is not possible to measure the individual default currents in each antenna terminal using the above experimental technique. In order to measure the power deposited in the plasma edge it is therefore necessary to excite the antenna in such a way that the default current enters through a single known terminal. The time averaged product of this current with the measured terminal voltage with respect to machine earth then gives the parasitic power.

This was achieved by grounding one side of the antenna so that all points along the antenna bars oscillate in phase. In this case, for a plasma of static potential, we may hypothesise that only the active side of the antenna sources a default current. A typical unintegrated default current is shown in Fig. 2b with the corresponding unintegrated terminal potential trace. Note that the second harmonic of Fig. 2a for the case of symmetric excitation has largely disappeared; in agreement with the hypothesis.

The default current in this experiment has half the amplitude of the circulating current since the antenna potential was fixed at DC earth. In this case the antenna never attains the negative polarisation necessary to reduce the large electron current on positive half-cycles of the oscillating potential to the value of the ion current on negative half-cycles and hence extinguish the DC current. As a result the power estimated is not directly relatable to that measured in the symmetric, floating antenna case. The power, 10 kW, calculated from the trace for this bar pair corresponds to a total antenna power between 20 and 30 kW assuming that the other outside bar pair behaves identically and depending on how much default current can be drawn along field lines by the centre bar pair. Unfortunately, due to the asymmetrical load, the normal AWH power measurement diagnostic was made nonoperational by this experiment so that a direct comparison is not available. Nonetheless, this magnitude of parasitic power would represent approximately 240 kW of wasted power if all eight antennae were excited asymmetrically in the same way with one terminal at machine earth. The AWH RF power is calculated by a voltage measurement across the symmetric RF power line and by a measurement of the average current in the line. This measurement is therefore expected to include the default current power.

The presence of some second harmonic on the default current with asymmetric excitation (Fig. 2b) is poorly understood, however unlike the first harmonic (2.04 MHz) the second harmonic is strongly fluctuating and varies considerably with plasma conditions. It could have two origins. The first is that the plasma potential oscillation produces a current component into the antenna. The second is that the second harmonic is a natural trait of the high voltage, high frequency Langmuir current effect in the SOL. In this case the characteristic can be checked by disconnecting completely one side of the antenna so that no circulating current flows and the antenna potential is uniform along the length of the antenna

bars. The fact that the default current flows from one terminal to the plasma can be checked by measuring the harmonics of the individual Rogowski currents.

The difference in the amplitude of the observed default current signals in the symmetric and asymmetric excitation experiments may be due to the natural polarisation of the antenna in the symmetric case and the non polarisation in the asymmetric case. It may also be due to the fact that a good portion of the first harmonic of the default currents flowing to the SOL in the symmetric case are cancelled during addition of the Rogowski signals.The natural polarisation of the antenna can be preserved during asymmetric experiments by connecting a low impedance capacitor from the antenna terminal to ground instead of making a direct connection. In this way one should obtain a default current of similar magnitude to that seen in the symmetric, floating antenna experiments.

During AWH with symmetrical excitation, harmonics have been observed on the magnetic wave field and ion saturation current signals in the SOL. The second harmonic (4.08 MHz) has been shown in some cases to be 50% of the fundamental signal. All harmoncs of the ion saturation current measured by a Langmuir probe, positioned far from the excited antenna, peak around the antenna radius. Such harmonics however have only been detected in the SOL. They have not been detected deeper in the plasma by the density fluctuation imaging diagnostic. Their level within the plasma does not exceed the sensitivity threshold of the Kinetic Alfven Wave amplitude at the applied frequency. It has been suggested [7] that these harmonics are due to the Langmuir effect at the antenna-SOL interface. An experiment with asymmetrical excitation has been performed in which the harmonics of the default current were measured as a function of the harmonics of the toroidal component of the magnetic wave field during an RF power scan. Since it is known that the amplitude of these harmonics all decrease with the negative level of artificial polarisation, the antenna was grounded as in the case of the default current power measurement to eliminate the effect of the antenna natural polarisation on the SOL. Asymmetrical excitation also permits excitation of a default current in a single antenna terminal to provide a single source of the plasma wavefields. It was predicted that the level of the harmonics (4.08, 5.12 and 8.16 MHz) of the plasma signal would increase linearly with those of the default current. Experiments however are still preliminary and have not yet provided clean enough signals for a valid comparison.

Conclusion Experimental results have been presented which form the first stage of a study of the plasma-antenna parasitic interaction during AWH in TCA. The results demonstrate that it is physically feasible to obtain a direct measurement of the power dissipated by the default current at the antenna-SOL interface and the measurement indicates that 20 - 30 kWs is delivered to the SOL in the particular case of the asymmetrically excited antenna when grounded directly at the machine earth.

Acknowledgements This work was partly supported by the Fonds National de la Recherche Scientifique.

References

[1] Weisen H. et. al., this conference.
[2] Collins G. A. et. al., (1986) Phys. Fluids 29, p. 2260.
[3] Joye B. et. al., (1988) Plas. Phys. and Contr. Fus. 30, p. 743.
[4] Appert K. et. al., (1987) Int. Conf. on Plas. Phys., Kiev.
[5] De Chambrier A. et. al., (1980) 4th Int. Symp. on Heating in Tor. Plas. Vol. 1., p. 193.
[6] Butler H.S. et al. (1963) Phys. Fluids 6, p. 1346.
[7] Dalla Piazza S. (1988) Rapport de Diplôme, Internal report CRPP-EPFL.

MEASUREMENTS OF THE TOKAMAK SAFETY FACTOR PROFILE BY MEANS OF DRIVEN RESONANT ALFVEN WAVES

H. Weisen, G.G. Borg, B. Joye, A.J. Knight, J.B. Lister

Centre de Recherches en Physique des Plasmas
Association Euratom – Confédération Suisse
Ecole Polytechnique Fédérale de Lausanne
21, av. des Bains, CH-1007 Lausanne/Switzerland

Alfvén waves are launched in the TCA tokamak (R, a = 0.61, 0.18 m, B_ϕ = 0.78–1.51 T, $I_p \leq 170$ kA and $n_e \leq 1.5 \times 10^{20}$ m^{-3}) by an external antenna structure [1]. An Alfvén resonance occurs wherever the local Alfvén velocity matches the externally imposed wave velocity, $\omega/k_{||}$. In the large aspect ratio approximation the resonance condition can be written as,

$$\omega^2 \rho(0) = K\,[n + m/q(r)]^2 \,/\, [\rho(r)/\rho(0)]\,, \tag{1}$$

where (n,m) are the toroidal and poloidal mode numbers respectively, $\rho(r)$ is the local mass density, and $q(r)$ is the local safety factor.

When the central line densities for which the resonance condition is satisfied at a given radius are known for two identical discharges, with, for example, (n,m) = (1,1) and (2,0) excitation, the local value of q can be obtained directly. To see this, we rewrite Eq. (1) as,

$$\omega^2 \rho_0\, \rho^*(r) \propto [n + m/q(r)]^2\,, \tag{2}$$

where ρ_0 is the central mass density and $\rho^*(r)$ is the mass density profile normalised to its value at r=0. We assume that $q(r)$ and $\rho^*(r)$ are independent of ρ_0. This allows us to write Eq. (2) with (n,m) = (1,1) and (2,0) and solve for the safety factor to obtain,

$$q(r) = \left[2(\rho_{01}/\rho_{02})^{1/2} - 1\right]^{-1}\,, \tag{3}$$

where ρ_{01} and ρ_{02} are the values of the central density when the (1,1) and the (2,0) modes are resonant at a given radius, r. The ratio of ρ_{01} and ρ_{02} can be obtained from electron line density measurements, assuming that the (1,1) and the (2,0) discharges have the same effective ion mass, $\rho(0)/n_e(0)$. To ensure this condition the ohmic discharge was disturbed as little as possible by using a minimal RF power.

The required mode numbers, (n,m) = (1,1) and (2,0), were determined by the relative phasing of the antennae and the RF power delivered to the plasma was 40 kW, at 2.04 MHz. The resonance positions were found by observing the associated density oscillations using a phase contrast imaging interferometer [2].

Figure 1 shows the radial profile of the amplitude and phase of the line density oscillation obtained for the same line averaged electron density in both the (1,1) and (2,0) continua. Although the two continua were observed to have the same threshold density, the (1,1) resonance layer appears at a larger radius than the (2,0) layer at this density, somewhat above the threshold, as a result of its dependence upon the safety factor. Figure 2 shows how the resonances moved to the plasma edge as the density increased.

Figure 3 shows the positions of the resonance layers for the (1,1) and (2,0) modes plotted as a function of line density measured for B_ϕ = 1.51 T and I_p = 125 kA. The difference in the rate of outward movement of the (1,1) and (2,0) resonances as the density increased illustrates the q dependence of the (1,1) layer. Although this discharge showed sawtooth behaviour, the ensuing modulation was not resolved in the measurements; the frequency response of the instrumentation provided an average over the sawtooth period.

Figure 4(a) shows the q profile deduced from the measurements of Fig. 3. As the density increase at low power was often insufficient to force the (2,0) resonance layer out to $r/a > 0.7$, we have added points at larger radii by using the Abel inverted density profile obtained from an eight chord far infrared interferometer (when available), together with the (1,1) resonance layer profiles. These are the filled circles in Fig. 4.

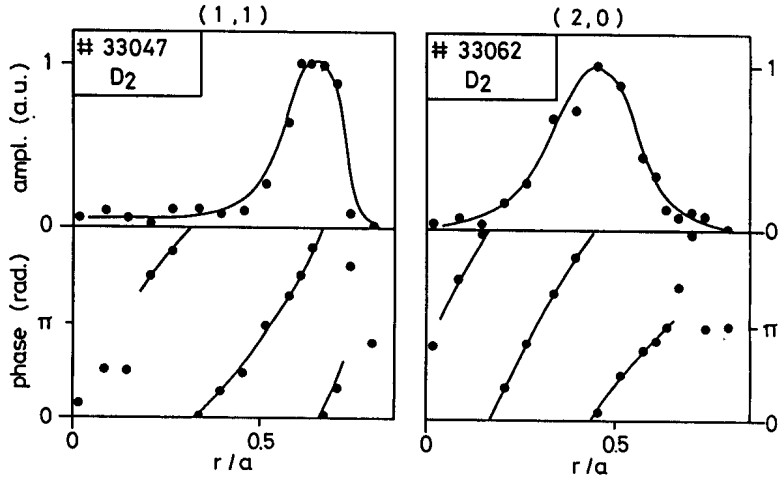

Fig. 1. Radial profiles of the synchronous line density oscillations obtained at the same values of line density and excitation frequency for (1,1) and (2,0) excitation.

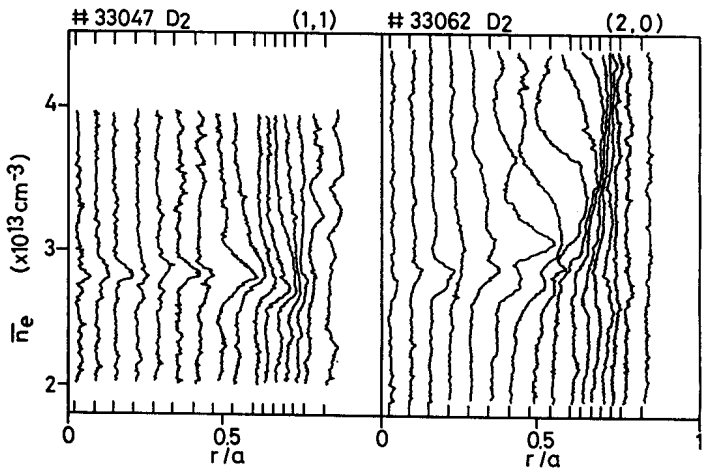

Fig 2. The density fluctuation amplitude plotted as a function of line density at 16 radial locations for the (1,1) and (2,0) discharges.

Figure 4(a) shows data taken from a sawtoothing discharge. This q profile is within a few percent of unity from $r/a = 0$ to $r/a \approx 0.4$, which corresponds, within one centimetre, to the sawtooth inversion radius obtained from soft x-ray measurements. The profile extrapolates well to the cylindrically equivalent safety factor at the edge, $q_I = 5\times10^6 a^2 B_\phi / R I_p$, in this case $q_I = 3.2$. The q_I values are indicated by the crosses in Fig.4.

Figures 4(b) and (c) show the q profiles for discharges with the same toroidal field as Fig. 4(a) but with plasma currents of 70 kA and 50 kA, respectively. Both these profiles also extrapolate well to the corresponding values of q_I, 5.7 and 7.9, respectively. These profiles do not have the flat central region shown in Fig. 4(a) and indicate a more peaked plasma current. Figure 4(b) shows q values in the central region slightly above unity, while 4(c) has central q values substantially above unity. Neither of these two discharges showed any sawtooth behaviour (the onset of sawteeth in TCA corresponds to $q_I \approx 5$).

Figure 4(d) shows the q profile for a discharge with a reduced toroidal field of $B_\phi = 1.16$ T and a larger plasma current of $I_p = 135$ kA. The reduced toroidal field, together

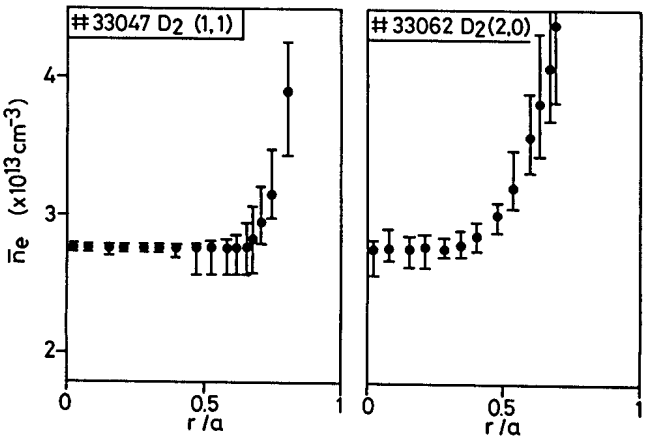

Fig. 3. Resonance layer positions for the (1,1) and (2,0) modes as a function of the central line density.

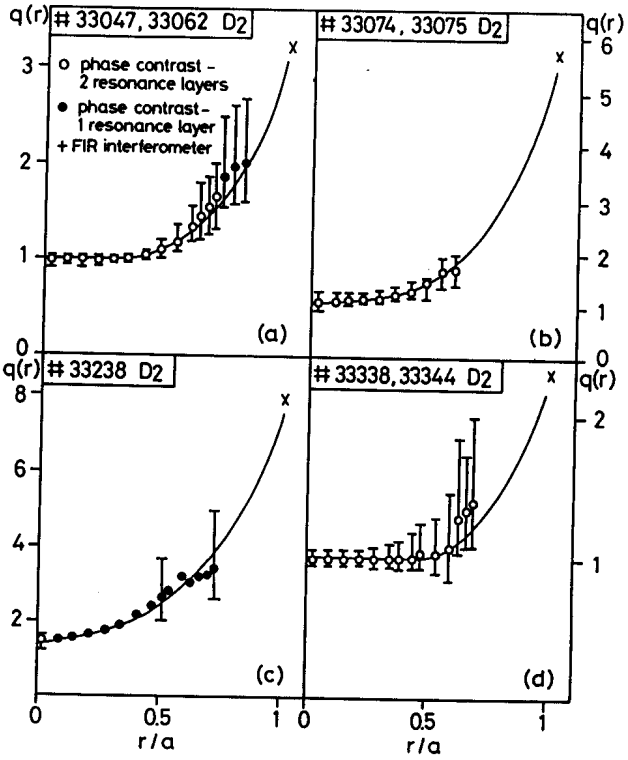

Fig. 4. Safety factor profiles for
(a) B_ϕ= 1.51 T, I_p = 125 kA,
(b) B_ϕ= 1.51 T, I_p = 70 kA,
(c) B_ϕ= 1.51 T, I_p = 50 kA,
(d) B_ϕ= 1.16 T, I_p = 135 kA.

with the higher plasma current, caused q_I to decrease to 2.3. Again, the measured q profile extrapolates well to this value. The reduced edge value of the safety factor was not associated with a reduced central value, compared to the case of Fig. 4(a). However, the central flat region has extended so that $q(r)$ stays close to unity out to $r/a \approx 0.5$. This distance corresponds to the increased sawtooth inversion radius observed on the soft x-ray signals.

Sawtooth resolved measurements show a strong modulation of the KAW phase and amplitude for $(n,m) = (2,0)$, equivalent to a 3% change in line density. The modulation by sawteeth is much weaker for $(n,m) = (1,1)$, suggesting that the change in mass density at the sawtooth collapse is compensated by the change in q. From Eq.(2) this suggests $\Delta q/q \approx -\Delta\rho/\rho \approx 3\%$, that is, the collapse expels a small amount of current together with the particles which carry the current.

Different techniques have so far yielded different measurements of $q(0)$. Our results indicate a flat q profile during sawteeth with q close to unity in the central region. This is consistent with the quasi-interchange sawtooth collapse model proposed by Wesson [3].

We are grateful for the support of the TCA team in this work, which was partly supported by the Fonds National Suisse de la Recherche Scientifique.

REFERENCES

[1] G.A. Collins et al., *Phys. Fluids*, **29**, 2260 (1986)
[2] H. Weisen, *Rev. Sci. Instrum.*, **59**, 1544 (1988)
[3] J.A. Wesson, *Plasma Phys. Contr. Fusion*, **28**, 243 (1986)

EFFECTS OF THE ALFVEN WAVE HEATING IN THE TCA TOKAMAK DEDUCED FROM THE PLASMA DYNAMICAL RESPONSE

Th. Dudok de Wit, B. Joye, J.B. Lister, J.-M. Moret

Centre de Recherches en Physique des Plasma, Association Euratom-Confédération Suisse
Ecole Polytechnique Fédérale de Lausanne
21, Av. des Bains, CH-1007 Lausanne, Switzerland

Alfvén wave heating as used on TCA has already been shown to have an important effect on most of the plasma parameters amongst which the most noticeable are the electron and ion temperatures, the kinetic energy content inferred from the diamagnetic flux, the Shafranov parameter $\Lambda = \beta_p + li/2 - 1$ deduced from the equilibrium vertical field and above all the plasma density. The spatial distribution of the resonant layers inherent in this kind of rf heating have been found to influence the temporal evolution of most of these parameters. This experimentally appears as a characteristic reduction of their time derivative at the same time as a new resonance layer appears in the plasma center. It is tempting to link these observations with a spatial redistribution of the absorbed power when the resonance surface structure is modified. Nevertheless the impressive density increase present during Alfvén wave heating makes the interpretation of these experiments somewhat difficult if we want to take into account these effects on an equivalent density variation for a purely ohmic shot.

Plasma dynamical response to Alfvén wave heating - Since our experiments are inherently transient, we chose to extensively study the dynamic plasma response [1]. TCA plasmas ($a = 0.18$ m, $R = 0.61$ m, $B_\varphi = 1.52$ T) are heated by Alfvén waves at 2.0 to 2.5 MHz launched by 8 phase-coherent antenna array. Dynamical response measurements were performed either by sinusoidally modulating or preprogramming one of the controlable machine parameter such as the rf power or the gas valve. The presented work concentrates on the study the response of the electron temperature in the range of modulation frequencies from 100 Hz to 500 Hz. At these frequencies both the density and the impurity content relative modulations remain much smaller than the soft-X-ray flux modulation. Thus the latter is attributed to a change in the electron temperature.

Profiles of the normalised gain and of the phase of the soft-X-ray response to a modulated rf power (Fig. 1) exhibit two distinct regions separated by a well defined radius. Inside this radius the temperature response profile displays the lowest gains and phases; outside both the gain and the phase increase. We note that that the modulated component of the soft X-ray signal comes mainly from a variation of the base line signal, although it will be shown that the sawtooth activity plays a important role in the electron temperature response. The presence of an electron thermal energy source associated with this perturbation is identified by the lowest value point on the phase profile, i.e. toward the inner side of the separation radius. At the highest studied frequencies, this thermal energy source lags the rf power by 180^o. This shows that the

electron temperature perturbation is not produced by directly thermalising the wave energy but by an indirect mechanism. Moreover, it has been possible to establish that this phase profile is independent of the resonance layer position. Two situations are shown in Fig. 1 where the resonant surface structure was modified by either a density or a frequency change. In the first case - low density or high frequency - all the resonance surfaces are in the plasma periphery while in the second case a new resonance layer has just appeared in the plasma center. Both conditions lead to the same, indistinguishable, phase profile. In fact, this same temperature response was produced by modulating the electron density with gas puffing in purely ohmic conditions. The apparent thermal energy source and the abrupt increase of the delay are associated with the q=1 surface and may be explained by modifications of the sawtooth activity. This unsuspected but natural reaction of the electron temperature to density variations is described in detail in a companion paper [2].

A comparison of the two cases presented in Fig. 1 shows that there is a significant difference in the electron temperature modulation amplitude. The relative gain is from 2 to 4 times bigger when all resonance layers are near the plasma edge compared with the case possessing a dominant central resonance surface. This considerable global decrease of the plasma response amplitude may well be the cause of the observed discontinuity in the time evolution of the plasma parameters when a new continuum is crossed. The unsuspected character of this observation should be emphasised : either gas puffing, producing mainly a modifiction of the edge density, or Alfvén wave heating, and the unavoidable presence of resonance surfaces in the plasma periphery, can induce a change in the energy content in the plasma bulk. With the available experimental results it is, however, not yet possible to determine whether this is the consequence of a modification of the density or the temperature in the plasma periphery.

Superposition of rf power and gas valve modulation - It has been previously established that most of the electron temperature variation during rf heating is an intrinsic reaction of the plasma to a change in the density. Under these circumstances it is obviously much more difficult to observe any experimental evidence of direct rf heating. Gas puffing may be used to control the density modulation due to the rf field. To achieve this the rf power and gas valve were modulated at the same frequency with a phase and amplitude relationship adjusted to minimise the line average density variation. This should leave an electron temperature modulated component which is directly driven by the modulated rf power. Figure 2 shows the amplitude profile of the soft-X-ray flux in three cases: with a modulation of the rf power only, with a modulation of the valve and finally with the described superposition. The experiment was caried out at 100 Hz with a maximum peak to peak rf power modulation limited to 20 kW by the gas valve dynamic range. Also indicated in the figure is the expected signal amplitude in the plasma center if this rf power was spacially uniformly absorbed. The central electron temperature response is compatible within the margin of error with a zero or a uniform heating although the plasma parameters and the heating scheme were set up so as to guarantee the presence of a resonance surface in the central part of the discharge. Only the outermost soft-X-ray channels displaid a larger residual oscillation. The phase of this oscillation with respect to the rf power is estimated to lie between 115^{o} and 140^{o}, a value which exceeds 90^{o} and which is incompatible with direct heating. It should be noted that it is difficult to guarantee that everywhere in the discharge the density variation was cancelled to a sufficiently low level since only the line integrated density modulation was minimised.

Discussion - In conclusion, although the presented experiments were designed to give the best chance to observe any direct electron heating by absorption of Alfvén waves, no clear answer was obtained. The error bar may be reduced by averaging results over many discharges which is hoped to be sufficient to resolve this question.

The theory of the Alfvén wave physics predicts that an inward propagating kinetic Alfvén wave is created by wave conversion at the resonance layer. This wave is then absorbed by Landau damping over a few wave lengths, quantitatively a few centimeters. The density perturbation associated with this wave has been observed and is in agreement with theory [3]. Quantitativly, if all of the coupled power were thermalised by this channel, a localised modulation of the electron temperature would have been visible. We are forced to consider the possibility of a large fraction of the rf power being dissipated by another mechanism. This could be explained by the very different ratio between the wave phase velocity and the electron thermal velocity in the edge and central part of the plasma column. This hypothesis is supported by the observation of improved heating at low plasma current where the electron temperature is smaller. Experiments will be carried out in a near future to see if this ratio is a key parameter in the processes of Alfvén wave thermalisation.

This work was supported in party by the Fonds National Suisse de la Recherche Scientifique.

References:

[1] B. Joye et al., Plasma Phys. and Contr. Fusion **30** (1988) 743.

[2] Th. Dudok de Wit et al., this conference.

[3] R. Behn et al., Plasma Phys. and Contr. Fusion **29** (1987) 75.

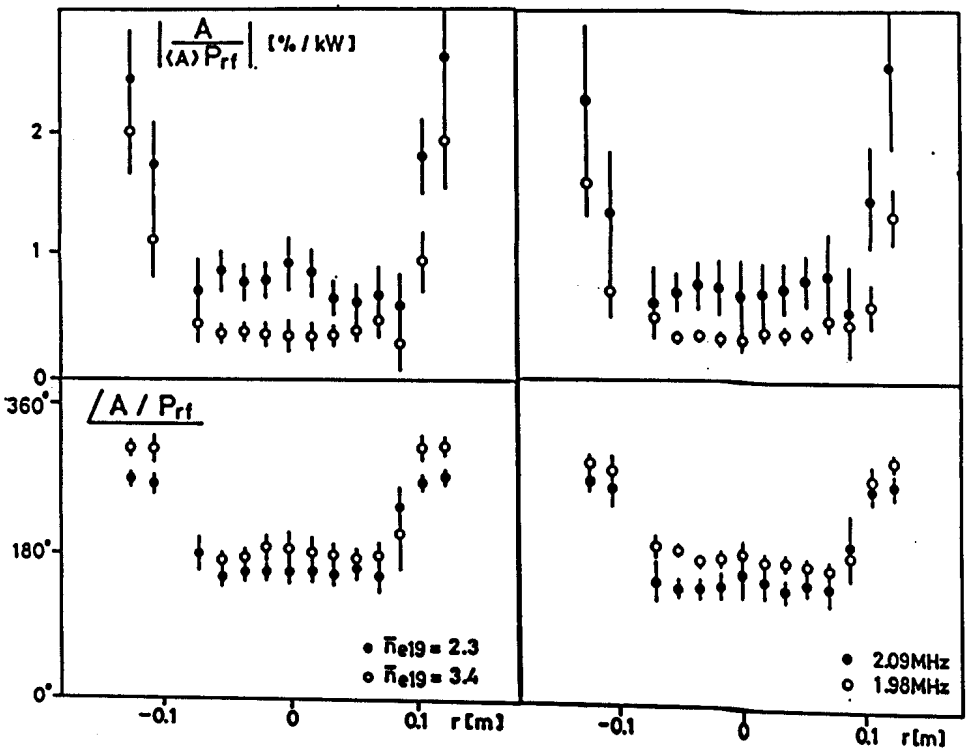

↑ Fig. 1 Relative gain and phase profile of the response of the Soft X-ray with RF modulation before and after crossing the DAW resonant surface a) by increasing the density, b) by increasing the Alfvén frequency.

↓ Fig. 2 Relative gain profile of the response of the Soft X-ray during either RF power modulation (o), gas valve modulation (•) or gas valve and power countermodulation resulting in a minimum density variation (+). The arrow gives the level of the expected amplitude for a uniform energy deposition.

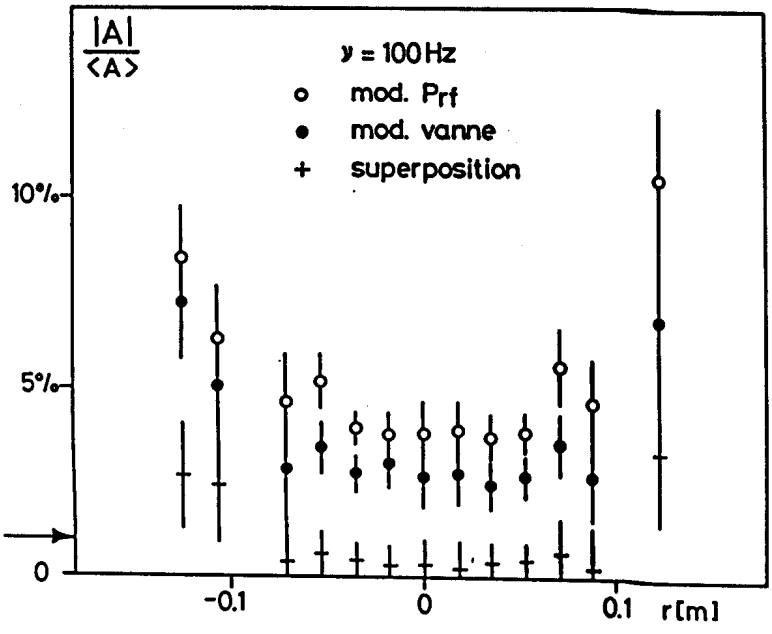

INVESTIGATION OF THE ENERGY TRANSPORT MECHANISM IN THE TCA TOKAMAK BY STUDYING THE PLASMA DYNAMICAL RESPONSE

Th. Dudok de Wit, B.P. Duval, B. Joye, J.B. Lister, J.-M. Moret

Centre de Recherches en Physique des Plasma, Association Euratom-Confédération Suisse
Ecole Polytechnique Fédérale de Lausanne
21, Av. des Bains, CH-1007 Lausanne, Switzerland

The energy transport mechanisms that govern the electron temperature behaviour of a tokamak remain very badly understood and up to now no proper model has been proposed that can explain experimental observations such as profile consistency or the influence of the density profile. One approach to this problem, extensively used on TCA, is to study the dynamical response of the plasma due to externally imposed modifications of parameters which have an influence on the plasma energy content. The temporal evolution of the electron temperature will closely depend on the type and the characteristics of the implied mechanisms. Thus a detailed measurement of the dynamical response would reveal experimentally the dominant properties that would have to be taken into account in the elaboration of a model of the transport processes.

Most of the results presented here were obtained by analysing the electron temperature response inferred from soft X-ray emissivity during modification of the plasma density due to either gas puffing, laser impurity ablation or Alfvén wave heating on TCA ($a = 0.18$ m, $R = 0.61$ m, $B_\phi = 1.52$ T), using the techniques described in [1].

Dynamical response of the electron temperature - Average plasma density has long been identified as an important parameter in the parametrisation of the global energy confinement time. And more recently the density profile has also shown a considerable effect [2]. The dynamical response of the electron temperature on TCA was first measured by sinusoidally modulating the gas valve between 30 and 300 Hz. Profiles of the relative amplitude and of the phase of the soft-X-ray response exhibit two distinct regions. The inner volume of the discharge displays the lowest gains and phases; outside a well-defined radius both the gain and the delay increase. Care was taken to ensure that the phase profile was continuous from low to high modulation frequency and that there were no unobserved 360° phase jumps. It has also been checked that throughout the discharge the relative density modulation is much smaller than the relative soft-X-ray modulation, guarantying that the observed effect is the consequence of an electron temperature variation. A plasma current scan between 55 kA and 125 kA clearly demonstrated that the surface separating the two regions is linked to the sawtooth inversion radius : results for 125 kA and 85 kA are plotted in Fig. 1. At the highest modulation frequencies used, the phase profile inside q=1 becomes slightly convex. Therefore, the outermost part of the inner region possesses the lowest phase, unambiguously indicating the presence here of an effective energy source. Surprisingly, the observed reaction of the electron temperature is not due to edge cooling by an influx of cold gas and another interpretation is required which will be discussed later.

Beside the dominant role played by the current profile via the q=1 radius in determining the electron temperature behaviour, it should be emphasised that the temporal evolution of the soft-X-ray emissivity can be exactly reproduced with several different perturbations : modification of the density by gas puffing, density increase following a short rf power pulse or reaction to injection of aluminium by laser ablation. In all these cases, the analysis of the temperature response leads to a transfert function in excellent agreement with the measured frequency response with harmonic modulation of the gas valve. Again we conclude that systematicly the sudden temperature decrease in the outermost observed region is not caused by radiation or cooling by new particles.

Variation of the current profile - Density modulation experiments are accompanied by a modulation of the Shafranov parameter $\Lambda = \beta_p + li/2 - 1$ measured via the vertical equilibrium field. Unfortunately, a diamagnetic measurement often used to determine the internal inductance, suffers from a vessel frequency cut-off and had to be discarded. Nevertheless, it is possible to have an idea of the current profile variation: Fig. 2 shows the complex amplitude of the modulated component of different parameters during a gas valve modulation at 100 Hz. The Shafranov parameter has been corrected for the vessel time constant. The density was chosen as the phase reference so that its amplitude is real. Also plotted is the modulation of the central soft-X-ray diode which is colinear with the central electron temperature amplitude. Due to the peakedness of the pressure profile, the β_p modulation must be close to a linear combination of both the density and the central electron temperature modulations with positive real coefficients. Thus the variation of the Shafranov parameter can only be explained if it is accompanied by a modification of the internal inductance and, therefore, of the current profile.

Influence on the sawtooth parameters - As the electron temperature response profile is essentially determined by the position of the q=1 surface, the sawtooth activity must have a considerable influence on its dynamic response. One should note that it is easy to achieve a variation of the base flux whose time derivative approaches or equals the sawtooth slope as seen in Fig. 4. Nevertheless, even under these circumstances, it has never been possible to observe zero or negative sawtooth slope in the plasma center. We see that most of the electron temperature variations are due to modifications in the sawtooth activity characteristics. The latter, namely the amplitude of the ramp, which is equal to the product of the slope and the period, and the amplitude of the crash, have been plotted on Fig. 3. In both cases the electron temperature response results from a net difference between the two quantities. More precisely, the same figure shows that the ramp amplitude variation is the consequence of a sawtooth period modification at constant slope which would not have been the case if the sawtooth signal were simply superposed on the base signal. The crash amplitude is found to be reduced during the central temperature rise and to greatly increase during the temperature drops. The opposite behaviour is observed outside the inversion radius where the small crashes lead to a reduction of the average electron temperature which can explain a 180^o phase shift in the phase profile.

Discussion - We shall now discuss the implications of the previous results on the modelling of the transport processes and their relation with other observations. To explain the observed dynamic response of the electron temperature, we require an apparent thermal energy source localised near the q=1 surface and an abrupt increase of the phase just outside this surface. This energy source may be due to magnetic to thermal energy exchange arising from the observed variation of the current distribution, and the large phase jumps could be attributed to a thermal insulation barrier associated

with the q=1 surface also observed during pellet injection in TFR [3]. These two features may be more conveniently produced by a variation of the thermal electron conductivity localised around the q=1 surface. This increase results in a local decrease of the outward heat flux, leading to an energy accumulation just inside and a lack of energy outside this region, thus producing an apparent energy source and a 180^{o} phase shift. Such a variation of the thermal energy diffusion coefficient during a transient was also used to simulate the evolution of the energy content at a ECH power step on TFR [4]. In an alternate model, the presence of an insulation layer in the q=1 region is supported by the lack of significativ central sawtooth slope variation even during very transient regimes, as if the plasma center were fully insulated from the outside. Here, an evolution of the time averaged central temperature is possible only if the elapsed time between crashes or their amplitude vary. When the crashes are small, there is an accumulation of thermal energy inside the q=1 surface but also a lack of energy outside the mixing radius to sustain the heat losses, producing a decrease of the peripheric temperature. It still remains unclear whether the determining parameter is the crash amplitude or the point at which the crash ends, two situations that would arise from quite different mechanisms.

The close link of these observations with the so-called profile resiliency has already been mentioned and is quite reasonable if one considers the role of the current profile in determining either the stationary temperature profile and its dynamical response profile. In addition, the systematic study of the electron temperature dynamic response has clearly established that the thermal insulation at the q=1 surface and the sawtooth activity characteristics are the most important elements in explaining the electron temperature behaviour and the energy transport in the plasma. This demonstates the power of such techniques in the investigation of the transport in a tokamak plasma.

This work was in part supported by the Fonds National Suisse de la Recherche Scientifique.

References

[1] J.-M. Moret, Thesis No 758, Ecole Polytechnique Fédérale de Lausanne, and Lausanne Research Paper LRP 358/88, October 1988.

[2] O. Gruber et al., Plasma Phys. and Contr. Fusion **30** (1988) 1611.

[3] TFR Group, 14th Europ. Conf. on Contr. Fusion and Plasma Physics, Madrid, Spain, 1987, Part I, Vol. 11D, p. 29.

[4] H.P.L. de Esch et al., Conf. on Contr. Fusion and Plasma Physics, Madrid, Spain, 1987, Part III, Vol. 11D, p. 876.

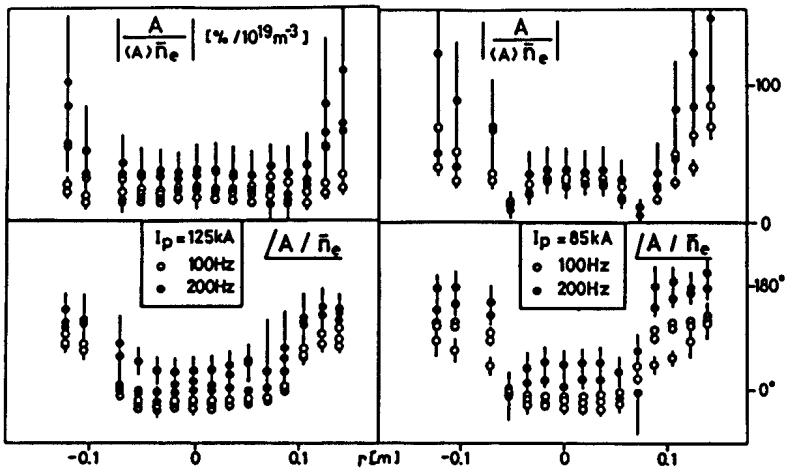

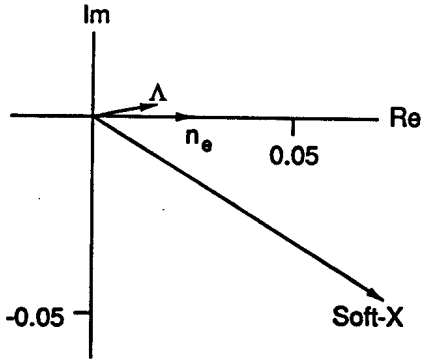

↑ **Fig. 1** Relative gain and phase profiles of the Soft X-ray response during gas valve modulation.

← **Fig. 2** Vector representation of the complex amplitude of the Shafranov parameter Λ during gas valve modulation.

↓ **Fig. 3** Raw Soft X-ray traces in and outside the inversion radius, during : a) RF power modulation, b) aluminium injection by laser ablation. The two upper graphs also show the sawtooth slope (--) and crash (--) amplitude. The lower graph gives the sawtooth frequency (--) and the time derivative of the slope at the center of the plasma (–).

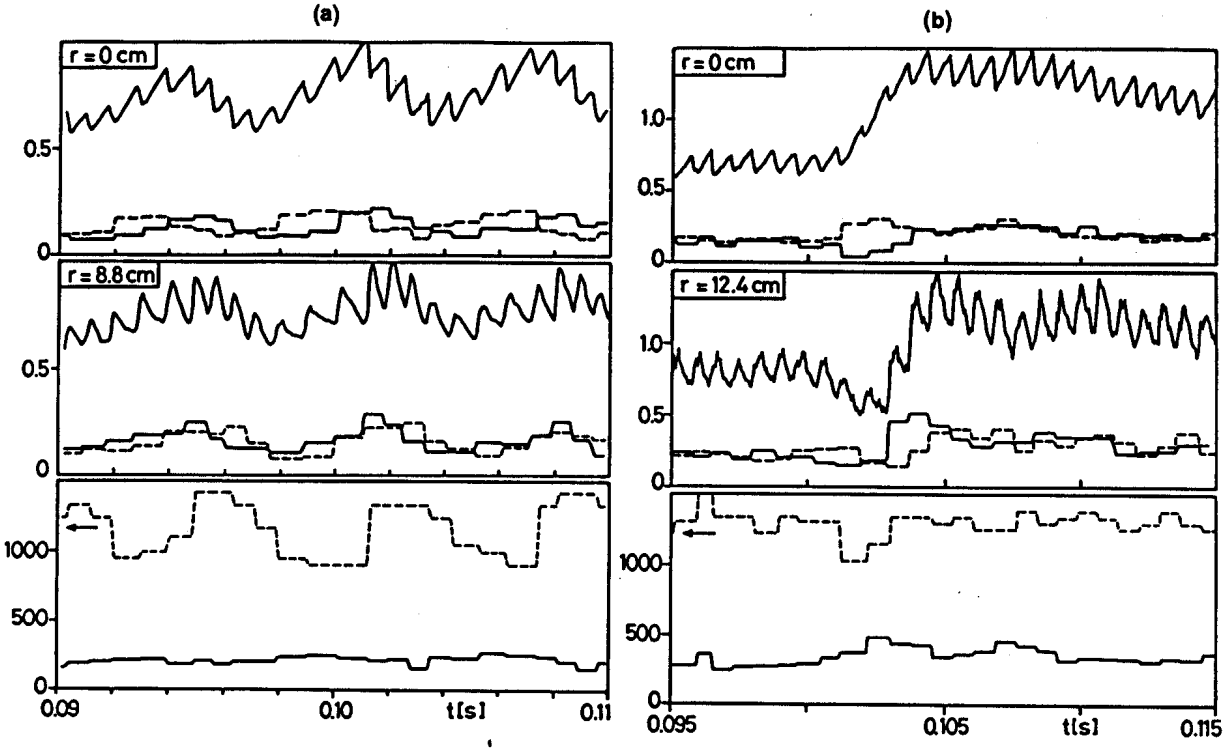

COMPARISON OF THE DRIVEN KINETIC ALFVEN WAVES OBSERVED IN THE TCA TOKAMAK WITH NUMERICAL SIMULATIONS.

K. Appert, G.G. Borg, B. Joye, A.J. Knight, J.B. Lister, J. Vaclavik, H. Weisen

Centre de Recherches en Physique des Plasmas
Association Euratom – Confédération Suisse
Ecole Polytechnique Fédérale de Lausanne
21, av. des Bains, CH-1007 Lausanne/Switzerland

INTRODUCTION

The TCA tokamak (R = 0.61m, a = 0.18m, $B_T \leq 1.5$ T, $n_e(0) \leq 1.8 \cdot 10^{20}$ m^{-3}, $I_p \leq 170$ kA) is equipped with four top-bottom antenna pairs to define the toroidal mode number n. An Alfvén resonance is excited whenever the local Alfvén velocity v_A matches the externally imposed wave velocity $\omega/k_{||}$. In the large aspect ratio approximation this condition can be written as

$$\omega^2\rho(r) = (n + m/q(r))^2 (B_T^2/\mu_0 R^2) (1 - \omega^2/\omega^2_{ci}) \qquad (1),$$

where ρ is the mass density and q the safety factor. Fig. 1 shows the resonance position as a function of the central density for two sets of mode numbers considered here, (n,m)=(2,0) and (-1,-1), with B_T = 1.5 T in a deuterium plasma, as relevant to our experimental conditions. The density profile was assumed to be parabolic and the current profile of the form $j(r) = j(0)(1-r^2/a^2)^{2.2}$ such that q(0)=1 and q(a)=3.2.

At high temperatures ($v_e \geq v_A$), kinetic theory predicts mode conversion at the resonance layer from the fast magnetosonic wave to a radially inward propagating wave with a large electrostatic component and an associated density perturbation[1]. The density modulation is detected using the phase contrast diagnostic installed on TCA[2]. It is similar to a laser imaging interferometer and is equipped with a 30 element HgCdTe infrared detector array and coherent amplification for 16 channels. Owing to the essentially cylindrical symmetry of the waves, the pattern of the line integrated density perturbation remains closely related to the original radial wave pattern. To a first approximation the local amplitude is multiplied by an effective integration length $L_{eff} = (2\pi r/k_r)^{0.5}$, where k_r is the radial wavenumber of the wave.

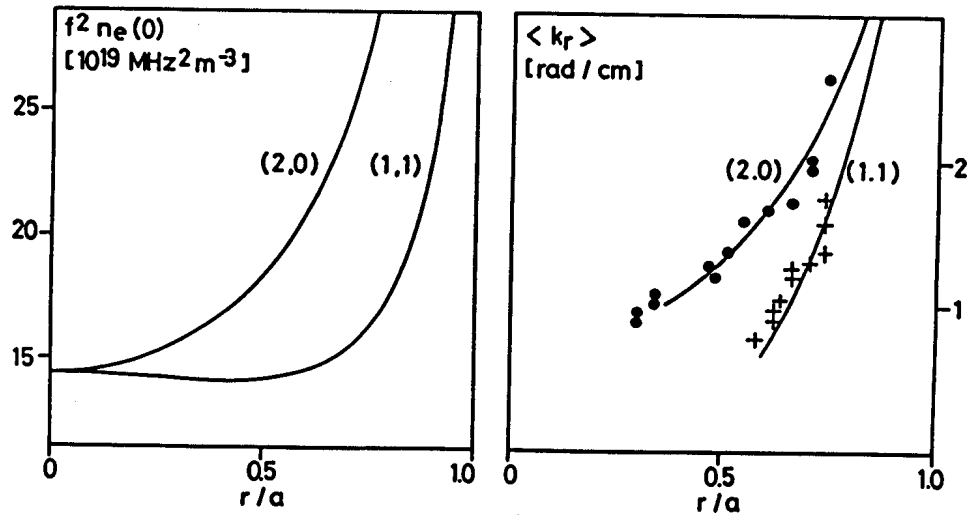

Fig. 1. Resonance curves for TCA conditions. Fig. 2 Mean radial wavenumber as function of position.

EXPERIMENTAL OBSERVATIONS

Fig. 3 shows examples of radial profiles of the amplitude and phase ($\psi(r)$) of the driven density fluctuations at different line densities with (n,m) = (-1,-1) and (2,0), and $P_{rf} \approx 40$ kW. At densities near the threshold below which the resonances are not in the plasma, the oscillations have the character of standing waves (constant phase profiles except for jumps of π). At higher densities they have a prevailingly propagating character (sloping phase profiles), with wavelengths that become shorter as the resonance layers move away from the plasma center. We shall only discuss the case of propagating waves in this paper.

Near resonance it is difficult to compare a local wavenumber ($d\psi/dr$) with theory because it varies rapidly from zero to a finite value. On fig. 2 we have instead plotted the average wavenumber $\langle k_r \rangle$ over the first cycle of inward propagation as a function of peak position. The solid lines were obtained from the approximate dispersion relation for the Kinetic Alfvén Wave expressed as

$$k_r \rho_i (3/4 + T_e/T_i)^{0.5} = ((\omega^2 - k_{||}^2 v_A^2)/ k_{||}^2 v_A^2))^{0.5} \qquad (2),$$

where ρ_i is the ion Larmor radius. The resonance profiles from fig. 1 were used together with a combined temperature profile $T_e + 3/4\ T_i$ assumed to be a parabola squared with a central value of 1 keV, in accordance with temperature measurements on TCA. Again $\langle k_r \rangle$ is an average over the first cycle and is plotted as a function of resonance position. The smaller $\langle k_r \rangle$ for (-1,-1) are a result of the shallowness of the (-1,-1) resonance profile. These waves remain closer to resonance and therefore maintain a longer wavelength. Propagating waves with wavenumbers significantly smaller than indicated on fig. 2 are not observed. Closer to

the thresholds only standing waves occur. In the conditions of the TCA tokamak, the KAW is predicted to be strongly electron Landau damped. The fractional damping rate $\delta_e = 1/2\ \pi^{1/2}\ v_a/v_e$ is in the range 0.2 (near the plasma centre where $T_e \approx 800$ eV) to 0.5 for a (-1,-1) KAW near r/a = 0.7 where $T_e \approx 200$ eV. This is in good agreement with our observation that the amplitude e-folding lengths estimated inward from the amplitude maxima are about one wavelength in the core region, but can be as small as 0.4 wavelength near r/a = 0.7.

COMPARISON WITH NUMERICAL CALCULATIONS

Numerical simulations of KAW excitation were performed in cylindrical geometry using the ISMENE kinetic code which includes Landau damping, transit time magnetic pumping and certain equilibrium gradient terms[3,4], and uses the formulation of Vaclavik[5] for the local power absorption. The profiles of plasma parameters used were similar to the above mentioned and the frequency was 2 MHz. Fig 4. shows profiles of local electron density fluctuation amplitude and phase for cases that can be compared to the corresponding examples on fig.3. Although there is a striking similarity between the wavefields observed and predicted by kinetic theory, exact matching of the two should not be expected because the details of the wavefields depend on the profiles of plasma parameters, and because fig.3 shows line integrated density oscillations. Absolute amplitudes for a given power agree within a factor of two. In the case of (n,m) = (2,0) direct excitation is poor. As a result the KAW amplitude on fig.4. c) and d) is not much larger than the fast (pump) wave amplitude, leading to oscillation profiles that are not representative of those obtained in a tokamak, where the (2,0) waves are excited efficiently via toroidal coupling by a (2,1) antennae structure. The experimental results should therefore be compared to the wave profiles shown as broken lines, where the fast wave component has been subtracted to show the (2,0) KAW only.

CONCLUSIONS

Experimental observations of the KAW in the TCA tokamak and numerical simulations using the ISMENE kinetic code are in excellent agreement. At a more basic level, the observed radial wavenumbers agree with the KAW dispersion relation. The attenuation of the wave amplitude is consistent with electron Landau damping.

This work was partly supported by the Swiss National Science Foundation.

References :

1. A. Hasegawa and L. Chen, Phys. Rev. Lett. **35** (1975), 370.
2. H. Weisen, Rev. Sci. Instrum. **59** (1988), 1544.
3. K. Appert et al., Int. Conf. on Plasma Physics, Kiev, **3** (1987), 172. Also LRP 319/87.
4. Th. Martin and J. Vaclavik, Helvetica Physica Acta **60** (1987), 471.
5. Vaclavik J. and Appert K., Plasma Phys. Contr. Fusion **29** (1987), 257.

Fig. 3 (left)

Experimental profiles of driven KAW's in TCA

Fig. 4 (right)

Simulated profiles of driven KAW's

a),b):
(n,m) = (-1,-1)
c),d):
(n,m) = (2,0)

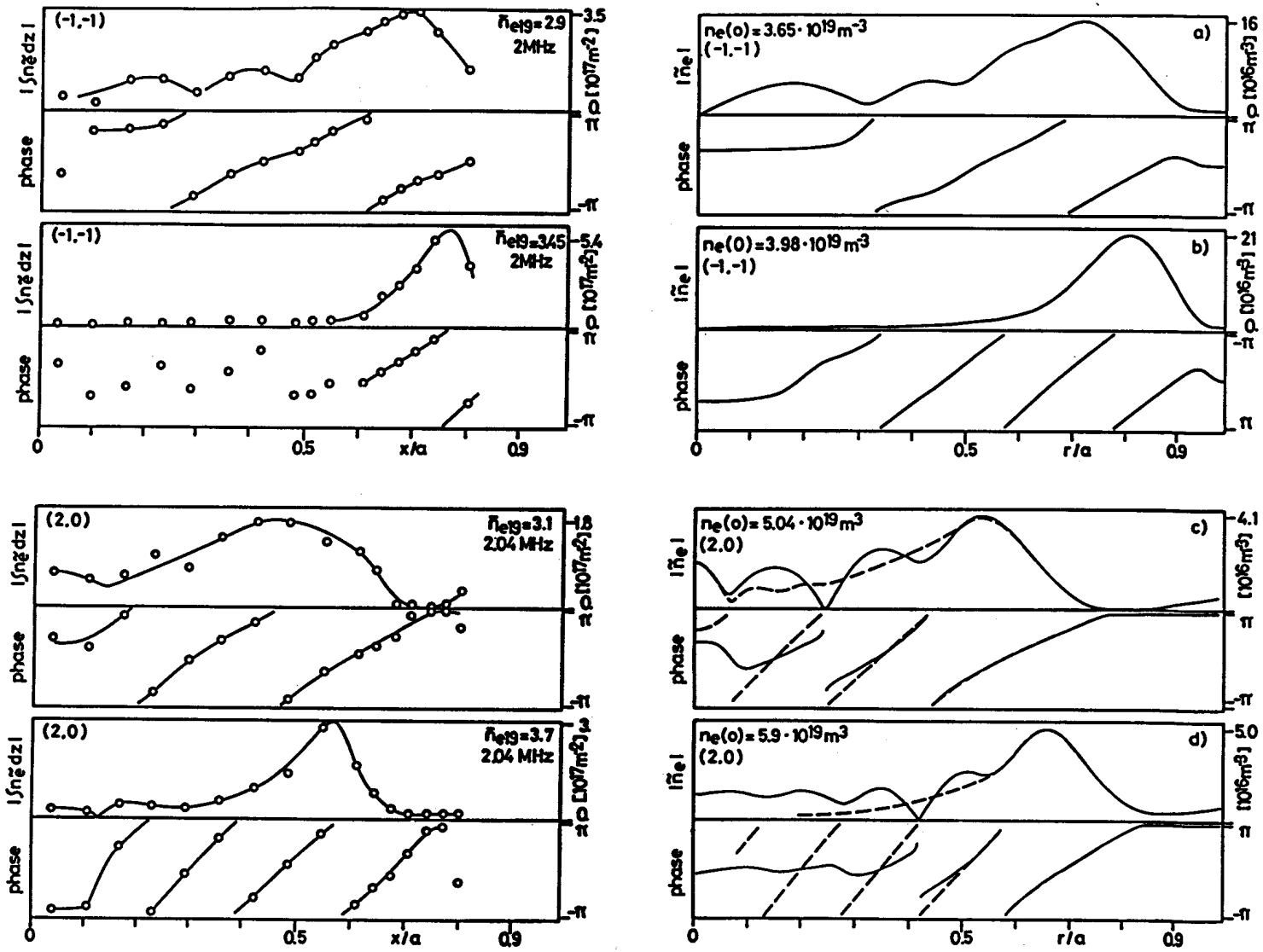

ION TEMPERATURE MEASUREMENTS OF H-, D- AND He-PLASMAS IN THE TCA TOKAMAK BY COLLECTIVE THOMSON SCATTERING OF D_2O LASER RADIATION

R. Behn, D. Dicken*, J. Hackmann*, S.A. Salito and M.R. Siegrist

Centre de Recherches en Physique des Plasmas
Association Euratom - Confédération Suisse
Ecole Polytechnique Fédérale de Lausanne
21, Av. des Bains CH-1007 Lausanne, Switzerland

*Permanent address: Institut für Laser- und Plasmaphysik, Universität Düsseldorf, F.R.G.

Development of collective Thomson scattering as a method to measure the ion temperature of a tokamak plasma has been successful and encouraging results have been obtained during experiments on TCA in H-, D- and He-plasmas. Using a laser source in the far-infrared spectral region allows scattering angles close to 90°, which results in excellent spatial resolution. The system installed on the TCA tokamak comprises an optically pumped D_2O laser emitting 0.5 J in a 1.4 μs pulse on its Raman transition at 385 μm. A heterodyne receiver with a Schottky barrier diode mixer has been chosen to detect the scattered radiation and analyze its spectral distribution in 12 channels of 80 MHz. Recent improvements of the mixer and 1st IF-amplifier yielded a system NEP of $2.2 \cdot 10^{-19}$ W/Hz. As a consequence we have obtained results which allow for the first time to evaluate the ion temperature T_i in a single laser shot.

Under the conditions of the scattering experiment on TCA the presence of impurity ions and the magnetic field were shown to have a noticeable influence on the shape of the spectrum. Fig.1 shows calculated spectra for parameters typical for a H-plasma in TCA. An example of a measured spectrum in hydrogen is presented in Fig.2. A value of $T_i = 330$ eV is found, using a standard curve fitting routine with the ion temperature T_i as the only free parameter. In order to determine the precision of a T_i measurement that can be obtained by our present set-up, a series of experiments under reproducible plasma conditions have been carried out in H-, D- and He-plasmas. The results are listed in Table I . A statistical analysis yields a standard deviation of 80 to 100 eV which corresponds to a relative error of about 25% . However, it should be mentioned that uncertainties in the other plasma parameters (especially Z_{eff}) provided as input to the fitting routine will lead to systematic errors. As long as the errors in T_e and N_e are less than 10% their influence on the evaluation of T_i is negligible.

During our first experiments a scattering geometry has been chosen where the difference wave vector $k = k_s - k_i$ is almost perpendicular to the vector of the total magnetic field $B = B_t + B_p$. Under these conditions a strong enhancement of the scattered intensity towards the centre of the spectrum is observed in agreement with the theoretical predictions. Although this influence can be taken into account by the fitting routine, the combined effect of the magnetic field and the impurity ions makes the interpretation of the spectra difficult, especially when the impurity content and Z_{eff} are not precisely known.

Therefore a second series of experiments has been carried out in a He-plasma after the geometry of the scattering experiment had been changed to avoid an orientation of k perpendicular to B (angle between $\underline{k}$ and $\underline{B}$: 86°). In He, as long as $T_e > T_i$, theory predicts a noticeable enhancement of the scattered intensity at a frequency corresponding to the ion-acoustic resonance. Under these conditions uncertainties in Z_{eff} do not strongly affect the shape of the spectrum in the region of interest and the evaluation of T_i is more precise. Fig. 3 shows a typical spectrum for a He- plasma in TCA; the fitting routine yields $T_i = 260$ eV.

The spectrum clearly shows the ion-acoustic feature in agreement with the theoretical model. As in the case of H- and D-plasmas we find a significant difference between T_e and T_i, which at present is not yet fully understood. The T_i-values from collective Thomson scattering are also systematically lower than those measured by a neutral particle analyzer (NPA). These observations will be subject to further investigations.

So far the experiments have demonstrated that collective Thomson scattering is a valuable method to measure the ion temperature of a tokamak plasma. The measured spectra are consistent with theoretical predictions assuming density fluctuations at the thermal level. The influence of the magnetic field can be avoided by a suitable choice of the scattering geometry. In the presence of light impurity ions (e.g. O and C) additional information about Z_{eff} is required to obtain optimum precision of a T_i measurement.

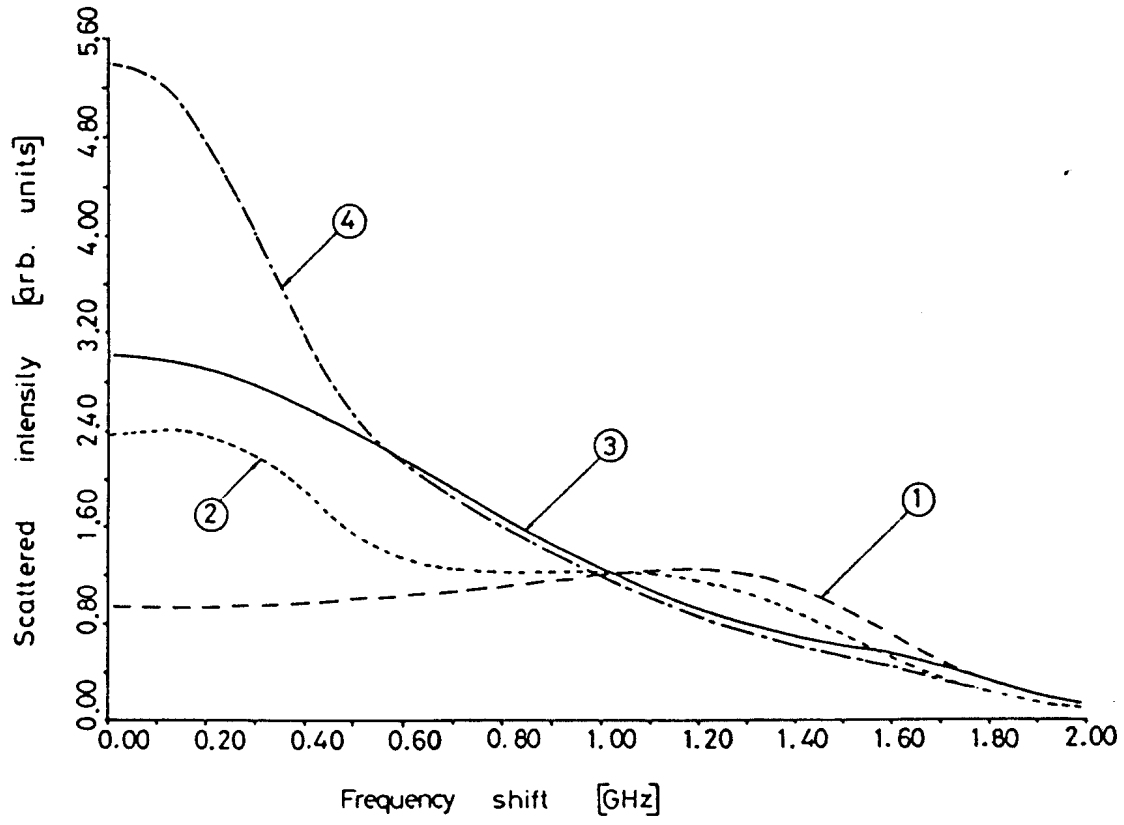

Fig. 1: **Calculated spectra for a H-plasma**
The 4 cases show the influence of the magnetic field and the impurity ions
Case 1: Basic spectrum (no magnetic field no impurities)
Case 2: Impurities included (Z_{eff}=2.5)
Case 3: Magnetic field included (B_t=1.5T, orientation 1° from normal)
Case 4: impurities and magnetic field included
Plasma parameters: $N_e=5.5*10^{19}m^{-3}$, T_e=680eV, Z_{eff}=2.5, B_t=1.5T

Table I Summary of T_i measurements

These results have been obtained during series of tokamak shots with reproducible plasma parameters. The standard deviation and the corresponding relative error value give an indication of the uncertainty of the measurement. However, it has been assumed that the other plasma parameters (N_e, T_e, Z_{eff} and β), required by the fitting procedure to evaluate T_i, are exact.

	H-Plasma	D-Plasma	He-Plasma
Ne	$5.5*10^{19}m^{-3}$	$5.3*10^{19}m^{-3}$	$5.0*10^{19}m^{-3}$
Te	680 eV	830 eV	600 eV
Zeff	2.5	2.5	2.7
Ti(fit)	250 eV	310 eV	380 eV
	320	450	430
	440	320	370
	230	460	410
	260	220	470
	370	300	260
	460	480	470
	300	490	270
	320	450	400
mean	330 (±30) eV	390 (±30) eV	390 (±25) eV
stand. dev.	80 eV	100 eV	80 eV
rel. error	25%	26%	20%

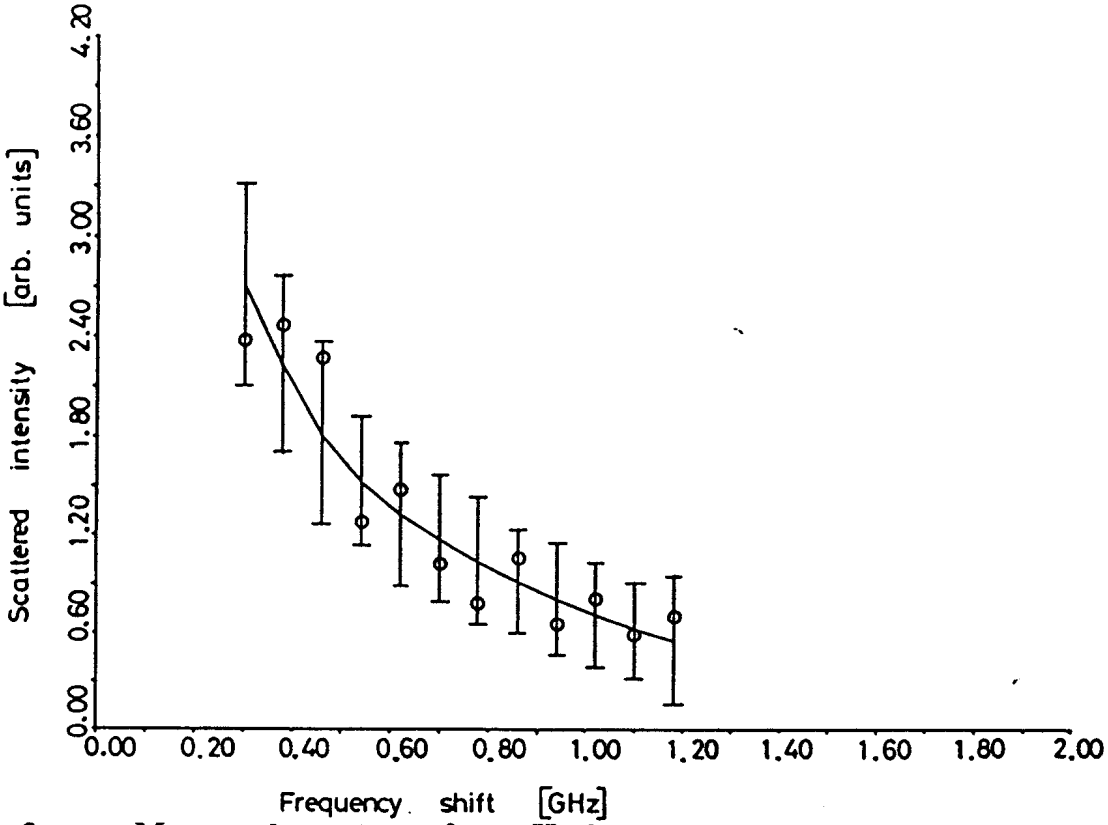

Fig. 2: **Measured spectrum for a H-plasma**
The spectrum is obtained from a single laser shot. The plasma parameters are:
$N_e = 7.9*10^{19}m^{-3}$, T_e=590 eV, Z_{eff}=2.5, B_t=1.5 T, angle ($\underline{k}$,$\underline{B}$)=89°.
The fitting procedures yields an ion temperature of T_i=330 eV.

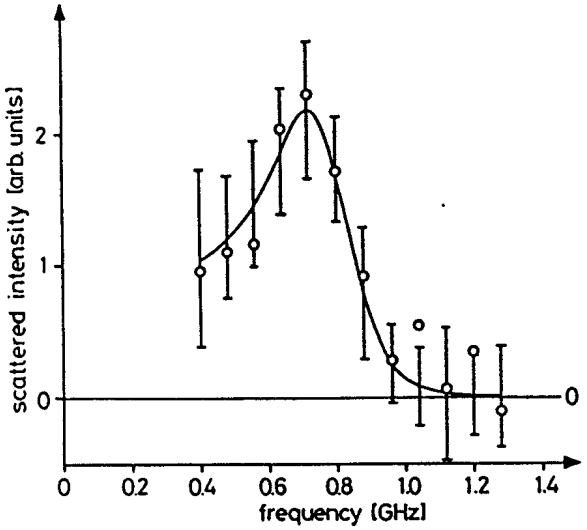

Fig. 3: **Measured spectrum for a He-plasma**
The spectrum is obtained from a single laser shot. The plasma parameters are:
$N_e=8*10^{19}m^{-3}$, T_e=620 eV, Z_{eff}=4.2, angle ($\underline{k}$,$\underline{B}$)=86°.
The fitting procedures yields an ion temperature of T_i=260 eV.

OPTIMIZED STARTUP OF ELONGATED PLASMAS IN THE TCV TOKAMAK

F. Hofmann, C. G. Schultz

Centre de Recherches en Physique des Plasmas
Association Euratom-Confédération Suisse
Ecole Polytechnique Fédérale de Lausanne
21, Avenue des Bains, CH 1007 Lausanne, Switzerland

1. Introduction

TCV is a new tokamak under construction at CRPP, Lausanne. It is designed to produce vertically elongated plasmas of various shapes with $I_p \leq 1.2$ MA and $\kappa \leq 3$. The optimal programming of shape evolution, plasma current and density rampup during the startup phase is a difficult problem. One of the difficulties stems from the fact that, in highly elongated plasmas, axisymmetric stability is favoured by low values of q_s [1], whereas kink stability requires relatively high values of q_s [2]. Whether the two stability domains can be made to overlap is not at all obvious. In this paper we consider a variety of startup scenarios, and we show that there are indeed classes of equilibria, with elongation $\kappa = 3$, which are both kink stable and whose vertical resistive growth rates are low enough to be stabilized by an active feedback system.

2. Vertical Instability Growth Rates with Resistive Walls

Under the assumption that the plasma is vertically stable with an ideally conducting shell, the time constant, τ_p , of the unstable motion in a resistive shell can be expressed as

$$\tau_s / \tau_p = \Omega_v^2 / \Omega_s^2 \qquad (1)$$

where τ_s is the resistive decay time of the induced currents in the shell (for the particular mode under consideration), Ω_s is the stable oscillation frequency of the plasma in a perfectly conducting shell, and Ω_v is the unstable growth rate in the vacuum field, without any shell. Eq.(1) implies that the effect of the poloidal field coils is negligible compared with the effect of the vacuum vessel, as is the case in TCV. Ω_s is computed by using the FBT code [3]. Approximate values of Ω_v can be obtained from

$$\Omega_v^2 = (2\pi R_0 I_p / M)\ (\partial B_R / \partial z) \qquad (2)$$

where R_0 is the major radius, I_p the plasma current, M the plasma mass and the radial field gradient is evaluated on the magnetic axis. The plasma mass, of course, also appears in Ω_s^2 and cancels out in Eq.(1). We note that, when the plasma approaches marginal stability on the fast time scale, Ω_s tends to zero and τ_s/τ_p diverges. In any given tokamak, τ_s/τ_p must be below a certain value, depending on machine parameters and on the bandwidth of the active feedback system. In TCV, $\tau_s = 6.7$ ms and τ_s/τ_p must be less than about 20.

3. Typical Startup Scenario

Let us consider a startup evolution in which a circular plasma is first created in the upper half of the vessel, close to the top wall. The shape then evolves according to a predetermined scenario (Fig.1), while current and density are ramped up simultaneously. Successive equilibria are generated as solutions of the Grad-Shafranov equation with the source functions:

$$p' = A + Bx^a + Cx^{a+1}$$
$$ff' = D + Ex + Fx^b + Gx^{b+1} \qquad (3)$$

where x is the normalized flux, $x = (\psi_{ax} - \psi)/(\psi_{ax} - \psi_{lim})$, ψ_{lim} and ψ_{ax} are the poloidal fluxes at the limiter and on the magnetic axis, respectively, and the constants a,b and A through G are assumed independent of elongation. In Fig.2a, we show the global plasma parameters as a function of elongation for a typical case. Current, pressure and q-profiles of the final plasma (κ=3) are also shown. The normalized vertical growth rate, τ_s/τ_p, is computed using the method described in the previous section. We consider two different versions of this scenario: The first is up-down asymmetric, as shown in Fig.1. The second version is up-down symmetric, i.e., the magnetic axis stays on the equatorial plane of the machine. We note that, in the asymmetric case, the maximum vertical growth rate is seen at the end of the scenario (κ=3), whereas in the symmetric case, the maximum appears at κ=2.6, and its value is twice the value at κ=3. In TCV, where normalized growth rates greater than 20 cannot be stabilized, the symmetric version of this scenario would be limited to κ=2.2. The asymmetric version, on the other hand, can go up to κ=3.

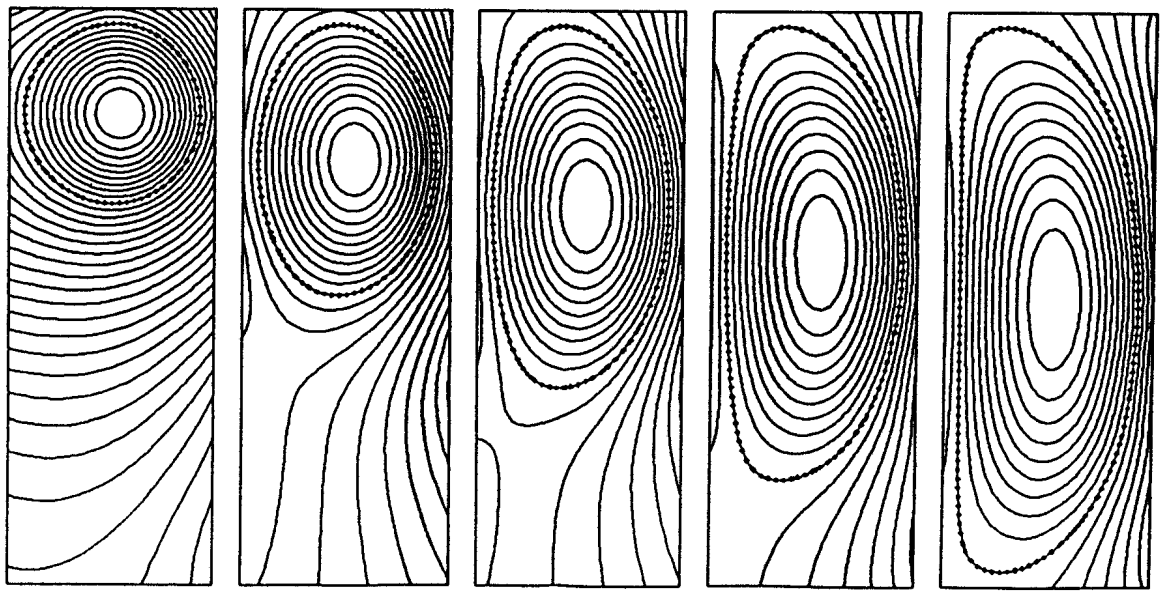

Fig.1. Typical plasma shape evolution during startup phase of TCV

4. Profile Optimization

A systematic study of the effects of profile variations has shown that, for a given plasma shape, the vertical growth rate depends primarily on two parameters, i.e., the internal inductance, l_i and the poloidal beta, β_p. For D-shaped plasmas with κ=3, the growth rate increases with increasing l_i, but it decreases with increasing β_p. This suggests that, from the point of view of axisymmetric stability, a high-beta startup is advantageous, i.e., the plasma density should be ramped up during, not after the current rise. Furthermore, we observe that, for given values of q_0, q_s and β_p, it is possible to reduce the vertical growth rate by modifying the current profile in such a way that l_i decreases. A startup scenario based on such current profiles is shown in Fig.2b. The shape evolution is the same as in Fig.1. Source functions are again assumed independent of elongation, and the current, pressure and q-profiles at κ=3 are also shown (Fig.2b). We note that the symmetric scenario now becomes feasible, since τ_s/τ_p <20. However, it is not at all clear whether current profiles such as the ones considered here can actually be produced in an experiment.

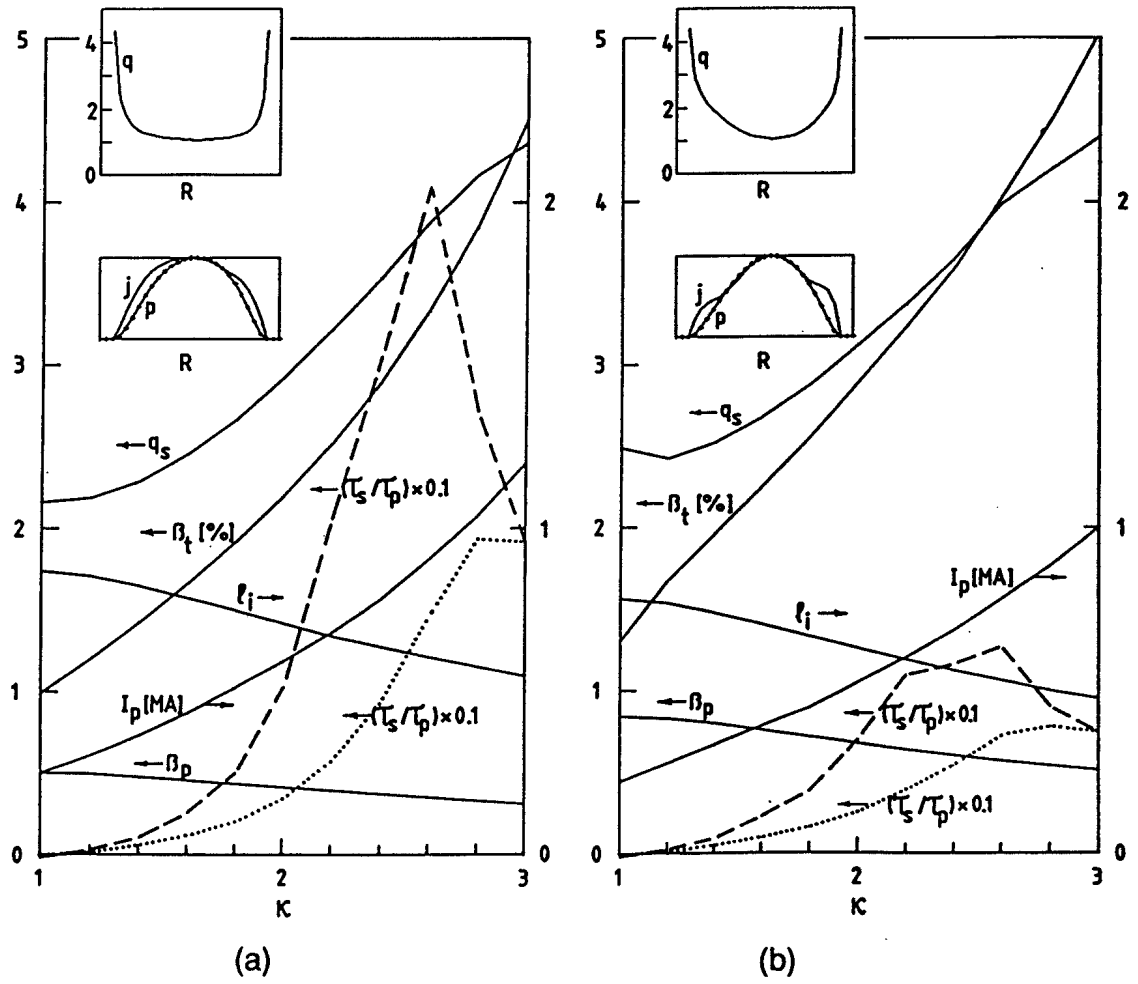

Fig.2. Global plasma parameters and vertical instability growth rates vs. elongation for up-down symmetric (dashed line) and asymmetric (dotted line) startup scenarios in TCV: (a) standard current profile, (b) bell-shaped current profile. q_0=1.05, B_0=1.5 T.

5. n=1 Kink Stability

In this section, we consider D-shaped plasmas with elongation $\kappa=3$, and triangularity $\delta^*=0.4$, corresponding to the rightmost equilibrium of Fig.1. We compute growth rates of the most unstable n=1 mode, using the ERATO code [4]. The effect of the conducting shell is not taken into account in these calculations. We assume $\beta=0$, $q_0=1.05$, $q_s=3.5$. The source functions are given in Eq.(3). A systematic parameter scan shows that, under these conditions, the n=1 growth rate depends essentially on the internal inductance, as shown in Fig.3. Note that n=1 growth rates below 10^{-4} are considered to be stable. It is interesting to see that n=1 stability is only possible in a narrow l_i-window, $0.42 < l_i < 0.46$. The n=0 vertical growth rates, τ_s/τ_p corresponding to this window, are far below the critical value of 20, and should be easily stabilized in TCV. The current profile in the n=1 stable range is very similar to the one shown in Fig.2b.

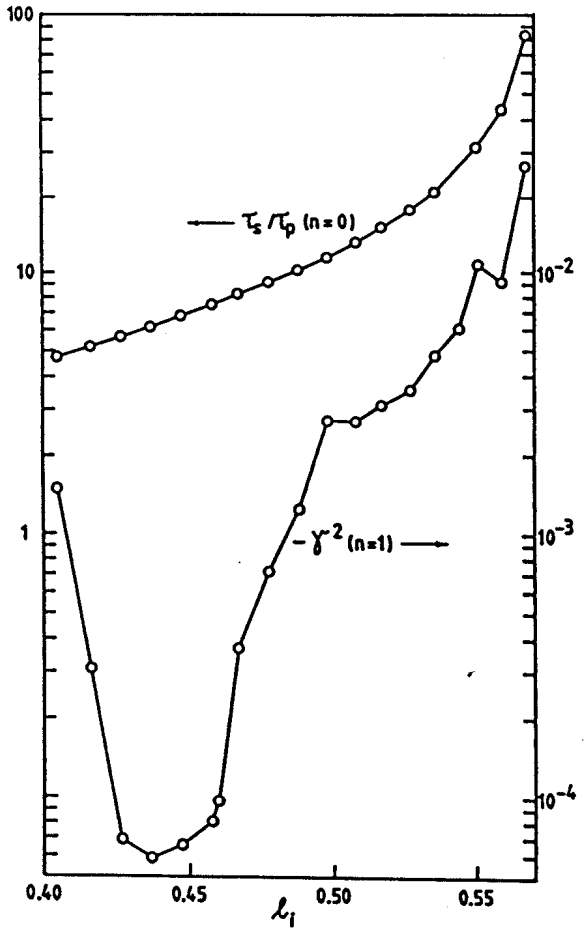

Fig.3. n=1 growth rate without shell (γ^2) and vertical growth rate with resistive shell (τ_s/τ_p) vs. l_i

6. Conclusions

The gain in axisymmetric stability resulting from an up-down asymmetric startup, as compared to a symmetric one, is important and perhaps crucial for reaching $\kappa=3$ in TCV. Resistive vertical growth rates can be reduced, at constant q_0 and q_s, by using bell-shaped current profiles. Finally, n=1 kink calculations for a D-shaped plasma with $\kappa=3$, $\beta=0$, $q_0=1.05$ and $q_s=3.5$ show that there is a stable window in l_i-space and that the corresponding n=0 vertical growth rates appear to be controllable in TCV.

Acknowledgements

Fruitful discussions with Professors A. Bondeson, F. Troyon and Drs. F.B. Marcus and G. Tonetti are gratefully acknowledged.

References

[1] Hofmann,F., Jardin,S.C., Marcus,F.B., Perez,A., Turnbull,A.D., Fusion Technology 1986 (Proc. 14th SOFT Avignon, 1986), I, 687 (Pergamon Press).
[2] Turnbull,A.D., Roy,A., Sauter,O., Troyon,F.S., Nucl. Fusion 28 (1988)1379.
[3] Hofmann, F., Comput. Phys. Commun. 48 (1988) 207.
[4] Gruber, R., et al., Comput. Phys. Commun. 21 (1981) 323.

Beta limits - MHD Stability Analysis for NET / ITER

C. G. Schultz, A. Bondeson, F. Troyon, A. Roy

Centre de Recherches en Physique des Plasmas
Association Euratom-Confédération Suisse
Ecole Polytechnique Fédérale de Lausanne
21, Avenue des Bains, CH 1007 Lausanne, Switzerland

1. Introduction

For the next generation of large Tokamaks, operation at β of a few percents is essential in order to reach ignition and maintain it. It has become accepted that only elongated cross-sections will allow the required β. The problems that remain are to quantify the gain brought by elongation and shaping and identify eventual penalties that might be associated with them such as reduced operational space, a greater sensitivity to the current profiles or even pathological current profiles which would require costly profile control systems.

The beneficial effect of elongation on β can be understood from the scaling law [1]

$$\beta[\%] < g\, l_N \ , \quad l_N = \mu_0 I / a B \qquad (1)$$

which gives the maximum value of β, derived from numerical optimizations, and which is found to reproduce well all the experimental data [1], with a g factor between 2.2 and 3.0. Higher elongations allow higher current I for a fixed plasma half-width a.

Here we report on an optimization in progress of the influence of triangularity δ and elongation κ on the ideal MHD β-limit for plasmas with a boundary specified by

$$r/a = A + \cos(\theta + \delta \sin\theta) \ , \quad z/a = \kappa \sin\theta \qquad (2)$$

The study is limited to free-boundary n=1 (kink) and n=∞ (ballooning) modes.

2. Profiles

Several studies have been made concerning the influence of triangularity on the ideal-MHD β-limit [3-7], however, the picture emerging from these studies is rather incoherent. It appears that the discrepancies are due to different choices of plasma profiles, in particular the pressure profile $p(\psi)$. To gain some understanding of the dependence on plasma profiles, we have carried out a detailed optimization of the pressure and current profiles for a noncircular plasma with κ=2 and δ=0.6. The study has been restricted to current profiles for which the surface averaged toroidal current I' is non-negative and vanishes at the plasma edge, and the safety factor q is everywhere above unity. (Note that the definition of I' differs from that used by Todd [5]).

In the circular case [8], the highest β-values are reached with a

top-hat current (Shafranov) profile with q_0 slightly above unity and low shear in the centre. The pressure gradients are localized in the external high-shear region where I'=0. With increasing triangularity, the optimum current profile remains essentially unchanged, however, the q-profile becomes rather strongly modified as $q(\psi)$ shoots up increasingly rapidly near the edge. An important effect of triangularity is to improve ballooning stability in the central region by a combination of increased shear and shaping.

Thus, for large triangularity, the optimum pressure profile has finite gradients in the central region of flat I', i.e., is more peaked than in the circular case. As the optimum profile depends on triangularity, it is clear that a full optimization must allow considerable freedom in $p(\psi)$ and that discrepancies between different β-limit studies have resulted from different restrictions on the pressure profiles. Furthermore, it is useful to specify the current rather than the q-profile, in particular, as the latter choice may lead to non-zero currents at the plasma edge, which strongly influences the stability of external modes.

A typical case of profiles $p'(\psi)$ and $I'(\psi)$ optimized for n=1 and n=∞ stability and κ=2, δ=0.6 is shown in Fig. 1. This case has q_0=1.07, q_s=4.2 and β=6% at an aspect ratio A=3.7. The current profile is somewhat broader than a top-hat, however, it is still flat in the centre and has I'=I''=0 at the edge. The pressure gradient in Fig. 1 is essentially proportional to the ballooning stability limit on each flux surface.

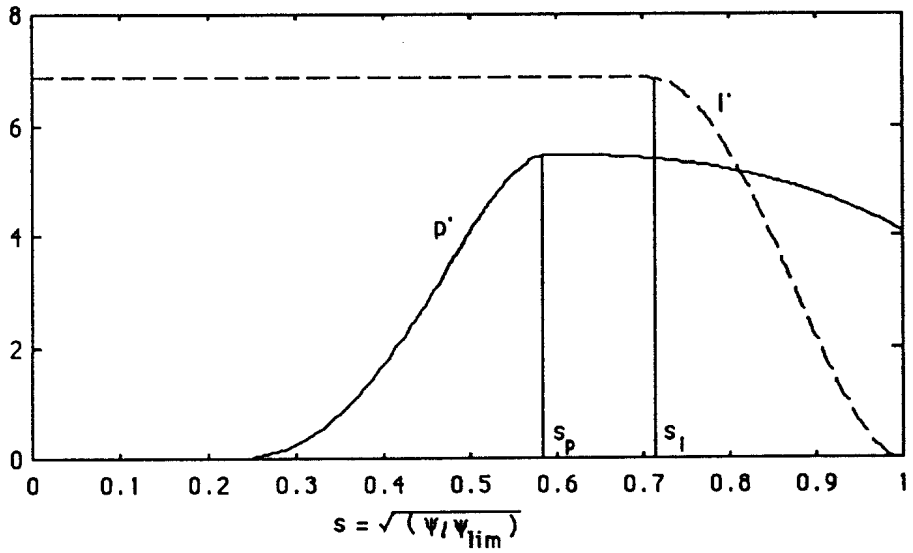

Fig. 1 Optimized pressure and current profiles for κ=2, δ=0.6, A=3.7 and β about 6%

3. Results $\beta_{max}(q_s,q_0)$ for δ=0.6 and κ=2

Using the ERATO stability code, we have computed the β-limit for equilibria of the type shown in Fig. 1, changing s_p and s_I. The result is shown in Fig. 2 as $\beta_{max}(q_s)$ for different values of q_0.

Several interesting features are seen in this diagram. The most striking result is that the β-limit is only weakly dependent on q_s between 2 and 5, in particular when q_0 is close to unity. Contrary to other studies [5,7] we do not find a pronounced deterioration of the β-limit for q_s<3, if q_0 is maintained close to unity. In addition, we note the absence of the so-called ravines observed in [5,7] when q_s is slightly below integer values. It appears that these two features depend on the choice of current

profile. For example, by comparison with cylindrical theory, we infer that the ravines are caused by finite current gradients I'' at the plasma surface. The sensitivity to the choice of current profile is well illustrated by the fact that the current profile in Fig. 1 avoids difficulty for $q_S<3$ as well as the ravines and instead gives rise to a β-limit which is very weakly dependent on q_S for $2<q_S<5$.

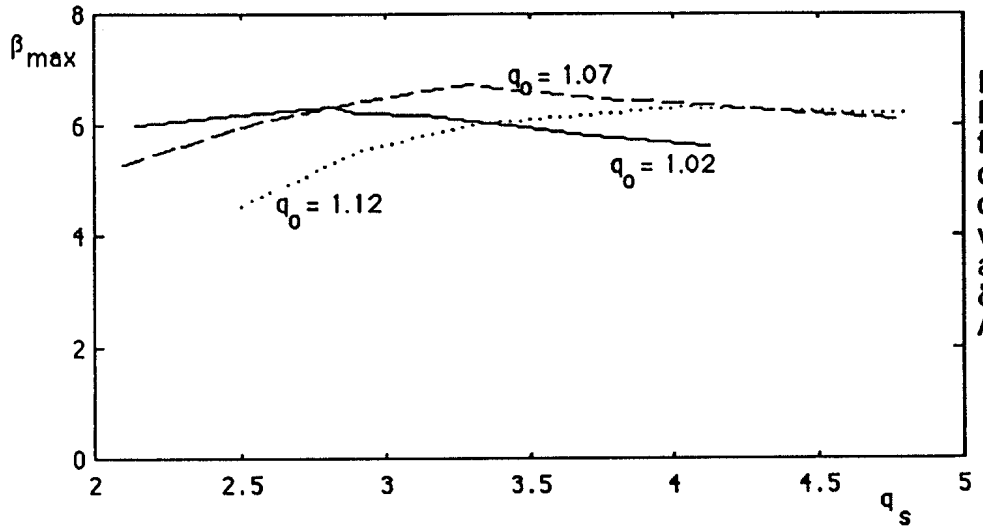

Fig. 2 Maximum β for varying q_S at three different values of q_0 and κ=2, δ=0.6 and A=3.7.

Since β_{max} is almost independent of the current in this range, g decreases with increasing current. At q_S=4.5, the maximal g reaches 3.0 The value for g is not decreased from the circular value even at the low values of q_S. We note that g comes out the same as for circular plasmas for which one has used the same kind of optimized current profiles [8], the values being higher than previously reported [1]. We also note that for $q_S>4$, the β-limit is not sensitive to the value of q_0. It is seen, however, that if q_0 is far above unity, the β-limit deteriorates at low q_S. The gain for an elongation of 2 has come in β: in the circular case one finds a maximum β of 2.5%, with κ=2 the maximum β is 6.7%, a gain by a factor of 2.7. At the same time the normalized current I_N has increased by a factor of 3 from the circular value.

From the particular case we have studied, κ=2 and δ=0.6, triangularity appears to open the possibility of operation at relatively high β and q_S at moderate current with a very high value of g without an excessive sensitivity to plasma conditions in the centre. Further studies of the dependence on ellipticity and triangularity as well as for the more realistic case of true free-boundary equilibria [9] are underway.

References

[1] Troyon, F., Gruber, R., Saurermann, H., Semenzato, S., Succi, S., Plasma Phys. Controlled Fusion 26 (1984) 209

[2] Stambaugh, R. et al., Plasma Phys. Controlled Fusion 30 (1988) 1585

[3] Todd, A.M.M., Manickam, J., Okabayashi, M., Chance, M.S., Grimm, R.C., Greene, J.M., Johnson, J.L., Nucl. Fusion 19 (1979) 743

[4] Yasseen, F., Cooper, W.A., Turnbull, A.D., Troyon, F., Roy, A., LRP 333/87 "MHD stability analysis for NET and INTOR", NET contract 242/86-6

[5] Phillips, M.W., Todd, A.M.M., Hughes, M.H., Manickam, J., Johnson, J.L., Parker, R.R., Nucl. Fusion 28 (1988) 1499

[6] Naitou, H., Yamazaki, K., Nucl. Fusion 28 (1988) 1751

[7] Hogan, J., presented at the ITER workshop on operational limits, IPP Garching, June 1988

[8] Roy, A., Troyon, F., "Ideal MHD stability of a circular cross-section tokamak", in Proceedings of the joint Varenna-Lausanne workshop on Theory of Fusion Plasmas, October 1988

[9] Hofmann, F., Schultz, C.G., these proceedings

HIGH DECAY INDEX PLASMAS IN DIII-D

J.B. Lister, J.-M. Moret, E.A. Lazarus*, A.G. Kellman+, T.S. Taylor+, J.R. Ferron+

Centre de Recherches en Physique des Plasmas
Association Euratom - Confédération Suisse
Ecole Polytechnique Fédérale de Lausanne
21, Av. des Bains, 1007 Lausanne, Switzerland

* Oak Ridge National Laboratory, P.O. Box Y, Oak Ridge, Tennesse 37831, U.S.A.
+ GA Technologies Inc. P.O. Box 81608, San Diego, California 92138, U.S.A.

The production of highly elongated plasmas requires large values of the vertical field decay index ($n=-R/B_Z\ dB_Z/dR$), which in turn render the plasma more and more difficult to maintain up to a critical decay index at which the plasma is ideally positionally unstable. In the DIII-D tokamak plasmas with n up to -0.96 were obtained with little trouble. This experimental limit was much lower than the predicted critical decay index. This paper describes the experiments carried out in order to study the vertical position problem in DIII-D, and the technique which was applied to stabilise high decay indices, up to ~-1.3, close to the predicted limit. This work prepares the way for the high plasma elongation which would be obtained with such a high decay index if the safety factor were also lower.

An approach to this problem has recently been evolved for improving the DIII-D tokamak vertical position feedback control [1]. The starting point for the model of the vertical stability dynamics is a rigid massless plasma which experiences a vertical force approximated as $F_V \sim I_p \times B_r(\text{axis})$. The vacuum vessel provides a restoring force via the radial field resulting from the image currents induced in it. The vessel currents are usefully decomposed into orthogonal modes, of which the first antisymmetric mode dominates, in the sense that both its coupling to the vertical movement and its decay time are largest. Active coils were added to the model in terms of their mutual inductance to the vessel current modes and their radial field at the plasma axis. Such a simple system as this leads to a low order dynamical system model, 2nd order when only one active pair of poloidal field control coils is considered.

Out of this very simple formulation, came the concept of hybrid vertical control. It was realised that no one active coil placement or control algorithm can usefully stabilise the vertical position. However, the hybrid system, in which the main, slower, radial field was provided by an outboard coil and a faster but weaker radial field was provided by inboard coils, seemed extremely promising, allowing the control of plasmas up to decay indices close to the ideal MHD positional stability limit with considerably reduced power requirements.

Experiments to study the stabilisation of high decay index plasmas were carried out on the DIII-D tokamak, R_0, a= 1.67, 0.67 m, B_ϕ = 2T, I_p = 1MA. The poloidal field system is extremely flexible, with 18 independantly controllable coils. The equilibrium field is programmed using all the coils, and the vertical position control is superimposed onto selected coils. The vertical position is detected using a combination of flux-loop signals and radial field coils.

The vertical feedback control was performed using two proportional plus derivative (PD) controllers (Gz+sGv) controlling either the F7 coils or the F7 and F2 coils

independently. A minimum number of active coils was used in order to reduce the imposed complexity of the control dynamics.

As a first step towards an understanding of the dynamical system which we must improve, we performed a set of perturbation injection experiments with a square-wave modulation (5Hz) introduced into the reference signal of the control loop. The vertical excursion was of the order 1-2 cm, ≈ 1% of the plasma height. We inspect the system response for three characteristic discharges. Figure 1a) shows a typical discharge. The response is damped, with a rise time of around 20msec. The controller in this case had a large value of $G_V \approx -10^{-2}$ and a large value of $G_Z = -2$. Figure 1b) shows an oscillating but damped response, still stable therefore, with much less velocity gain. Finally, Fig. 1c), we obtain an oscillatory but unstable discharge, with similar gains, but at a slightly larger decay index. The positive pole in the third case remains small, around $Re(s_1) \sim 10 sec^{-1}$, being vertically unstable in the closed loop control sense rather than the ideal MHD sense. In these three cases, there is no evidence of any difference between the response of the magnetic and soft X-ray measurements of the vertical position.

A system identification tool [2] was developed for dynamical studies on TCA. The modelling was carried out on the data of Fig. 1a), averaging 3 square-wave cycles to increase the signal-to-noise ratio. The results in Fig. 2 show the measured response, dashed curve, and the modelled response, solid curve, to the square wave stimulus also shown. The model agreement improves as the determinant order increases to second order, after which the character is barely modified by the presence of more degrees of freedom. This saturation is seen in the correlation coefficient which increases up to a second order denominator. The pronounced characteristic knee when the model order exceeds the identified system order is frequently used as a criterion to choose the optimum model structure. Since the experimentally observed behaviour of the vertical position control loop is that of a low order system, we should be able to model it with a low order model such as the three determining equations which were derived in [1]. The control strategy should be developed within the framework of this simple model.

A series of discharges was run to check the controller action. When both proportional and derivative controller gains are varied, the behaviour of the square wave response was in qualitative agreement with the model.

As the vertical field decay index is increased, the results of [1] predicted an increase in the more dangerous root of the transfer function, and subsequent loss of control at a certain decay index. Above the coil critical decay index, n_a, there is no stabilised solution without derivative gain, and above the vacuum vessel decay index, n_c, there is no stabilised solution at all. Prior to this systematic study, the loss of vertical control had always occurred in DIII-D at a decay index of $n_a = -0.95$, well below the value of $n_c = -1.35$ which was calculated for the discharges studied, but close to the coil critical decay index. Figure 3 shows the square-wave response as the decay index is ramped from $n \approx 0.8$ to $n \approx -1.1$, with the controller gains set at $-G_Z = 0.20$, $-G_V = 1.0$. The response at the start of the ramp shows very little overshoot, being roughly critically damped ($t \approx 1.3$ sec.). As the decay index increases negatively, the response starts to overshoot ($t \approx 1.5$ sec.) and by $t \approx 1.7$ sec. the response is oscillatory. The oscillatory nature increases, corresponding to a more inertial system until at $t = 2.1$ sec the oscillation becomes unstable and a disruption ensues. In this one discharge we have seen the characteristic behaviour predicted in [1], namely that of a low order system whose stability boundaries are moving as the decay index varies.

Since the G_Z, G_V settings determine the closed-loop poles, we expect the operational range to vary with the gains. Figure 4 shows three discharges (crosses) which were obtained

by increasing G_V. In each case we measure the maximum value of the decay index achieved just before the disruption, and plot this value against the velocity gain used. The decay index achieved increased significantly following the addition of a significant derivative gain, from - 0.96 to - 1.16. Between G_V = - 3 and G_V = - 10 little improvement was found, as predicted. The value of n = - 1.16 was the limiting value calculated for vertical control by the F7 coils, and is well below the critical decay index of the vacuum vessel for these discharges ($n_c \sim 1.35$).

The hybrid control was tested on the same series of discharges for comparison, and the results are illustrated in Fig. 4. Adding only derivative feedback to the F2 coils (G_{VF}), a value of n = - 1.18 was achieved at low G_V = - 0.1. This already exceeded the F7 coil optimum, n = - 1.16. Increasing G_V to - 10, the velocity feedback on the F2 coils still produced a significant increase in the decay index, up to 97 % of the calculated maximum, shown by the asterisks and rectangle.

These data show that the predictions of a simple vertical control model can lead to significant improvements in the achieved decay index, by providing a simple clear picture of the controlled system. Such an improvement was in addition obtained with a small amount of experimental data, contrary to the habitual trial and error optimisation.

The aim of the control optimisation was to achieve the higher plasma elongations which result from the higher decay indices. This series of discharges was run in abnormally dirty, high q, i.e. high l_i, conditions. When l_i is large, $\approx$ 1.4, the decay index necessary to achieve high elongation, K > 2.5, exceeds the vessel critical decay index. However, the elongation achieved with hybrid control, up to K = 2.38, exceeded previous attempts.

Acknowledgement - Two of the authors (E.A. Lazarus and J.B. Lister) would like to thank Ron Stambaugh, Tony Taylor and the DIII-D physics staff for their hospitality during their detachment at General Atomics. The work described was partly funded by the Fonds National Suisse de la Recherche Scientifique.

REFERENCES

[1] LAZARUS, E.A., LISTER, J.B, NIELSON, G.H., to be published
[2] MORET, J.M., Thesis No. 758, EPFL, Switzerland. Lausanne Research Paper LRP 258/88.

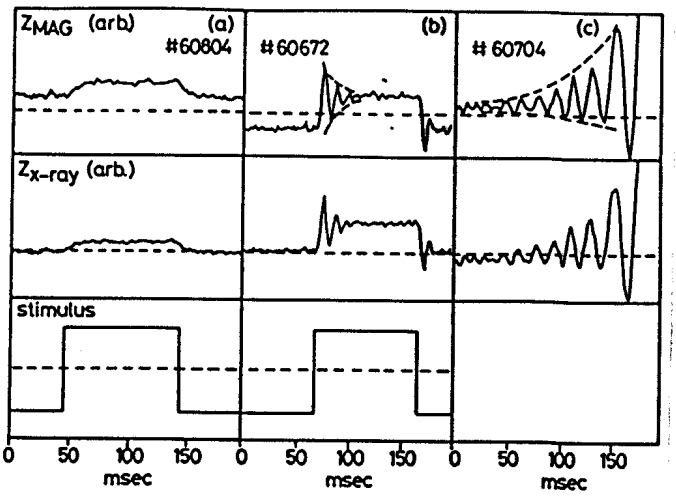

Fig. 1: Square-Wave Responses
a) overdamped **b)** underdamped
c) unstable oscillatory

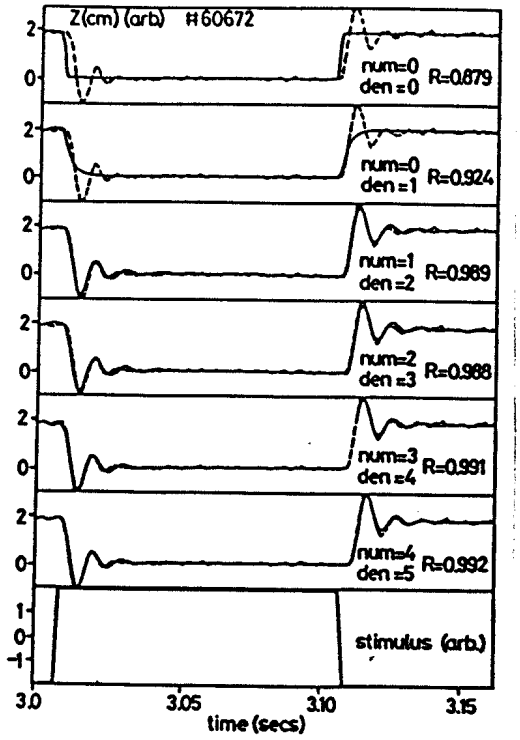

Fig. 2: Low-order dynamic modelling

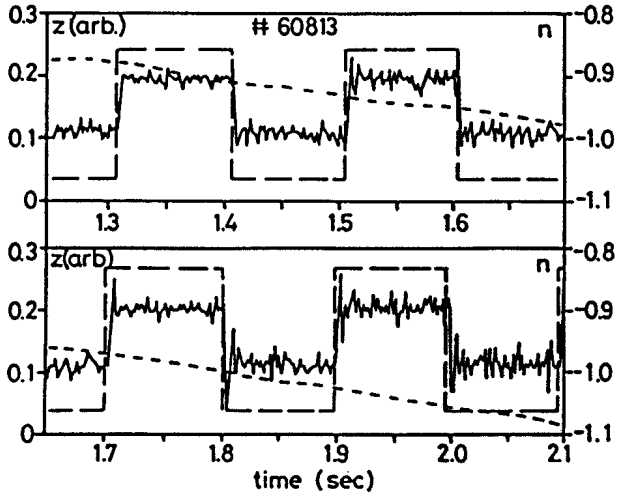

Fig. 3: Varying response during n-ramp

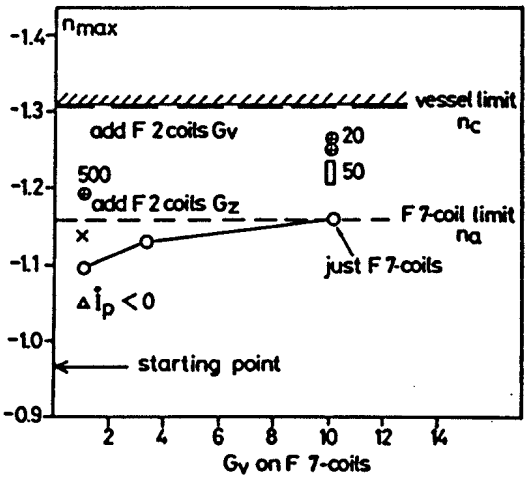

Fig. 4: Improvements with hybrid control